NEUTRON DIFFRACTION STUDIES OF SOME

RARE EARTH-TRANSITION METAL DEUTERIDES

FINAL REPORT

William J. James

May 1986

U. S. Army Research Office

DAAG29-83-K-0159

Graduate Center for Materials Research

University of Missouri - Rolla

Rolla, MO 65401

APPROVED FOR PUBLIC RELEASE;

DISTRIBUTION UNLIMITED

REPORT DOCUMENTATION PAGE		READ INSTRUCTIONS BEFORE COMPLETING FORM
1. REPORT NUMBER ARO 19783.4-MS	**2. GOVT ACCESSION NO.**	**3. RECIPIENT'S CATALOG NUMBER**
4. TITLE *(and Subtitle)* NEUTRON DIFFRACTION STUDIES OF SOME RARE EARTH- TRANSITION METAL DEUTERIDES		**5. TYPE OF REPORT & PERIOD COVERED** Final 11/15/83 - 12/01/85
		6. PERFORMING ORG. REPORT NUMBER
7. AUTHOR(s) William J. James		**8. CONTRACT OR GRANT NUMBER(s)** DAAG29 83 K 0159
9. PERFORMING ORGANIZATION NAME AND ADDRESS Graduate Center for Materials Research University of Missouri-Rolla Rolla, MO 65401		**10. PROGRAM ELEMENT, PROJECT, TASK AREA & WORK UNIT NUMBERS**
11. CONTROLLING OFFICE NAME AND ADDRESS U. S. Army Research Office Post Office Box 12211 Research Triangle Park, NC 27709		**12. REPORT DATE** May 1986
		13. NUMBER OF PAGES
14. MONITORING AGENCY NAME & ADDRESS(*If different from Controlling Office*)		**15. SECURITY CLASS.** *(of this report)* Unclassified
		15a. DECLASSIFICATION/DOWNGRADING SCHEDULE

16. DISTRIBUTION STATEMENT *(of this Report)*

Approved for public release; distribution
unlimited.

17. DISTRIBUTION STATEMENT *(of the abstract entered in Block 20, If different from Report)*

NA

18. SUPPLEMENTARY NOTES

THE VIEW, OPINIONS, AND/OR FINDINGS CONTAINED IN THIS REPORT
ARE THOSE OF THE AUTHOR(S) AND SHOULD NOT BE CONSTRUED AS
AN OFFICIAL DEPARTMENT OF THE ARMY POSITION, POLICY, OR DE-
CISION, UNLESS SO DESIGNATED BY OTHER DOCUMENTATION.

19. KEY WORDS *(Continue on reverse side if necessary and identify by block number)*

neutron diffraction - magnetic structure - rare earth-transition metal alloys
and hydrides, permanent magnets, sublattice,

Mu sub B

20. ABSTRACT *(Continue on reverse side if necessary and identify by block number)*

Neutron diffraction experiments were performed on Ho_6Mn_{23}. At 77K it is
found to have a face-centered cubic crystal structure and a non-collinear
magnetic structure, with the Ho moments tilted at an angle of 33.4° to the Mn
moments. The Ho atom carries a moment of $3.8\mu_B$, while the Mn moments at the
b, d, f_1 and f_2 sites are 2.1, 2.0, 2.2 and 1.9μ_B respectively, comparable
to those found in Y_6Mn_{23}. The very low moment on the Ho atom is rationalized
as resulting from the fanning of the weakly coupled rare earth moments around
the net Ho moment direction, giving a low spatially averaged value. Powder

DD _{1 JAN 73} **1473** EDITION OF 1 NOV 65 IS OBSOLETE

20 neutron diffraction data for $Ho_6Mn_{23}D_{22}$ were analyzed by a modified Rietveld technique. At 298K the space group is Fm3m; at 9K, P4/mmm. At 298K the deuteriums occupy the a, f_3, j, and k sites, in agreement with the predictions of Westlake's model. At 9K, a noncollinear antiferromagnetic structure is found, with Ho moments of approximately $3.5 \mu_B$/atom on all sites. The unusually low moment on the Ho atom is attributed to two effects; a low spatial average for the Ho moment in the Ho_6Mn_{23} compound and a further lowering upon deuteration of the compound, probably arising from disorder caused by the significantly lower ordering temperature. Neutron diffraction studies of three $Y_6(Fe_{1-x}Al_x)_{23}$ compounds (x=0.05, 0.10, 0.15) at 523K and 77K reveal substantial preferential atomic ordering of Fe and Al atoms on the four transition crystallographic sites. Fe atoms prefer to occupy the f_1 site and Al atoms the f_2 site. The site preferences are explained on the basis of the comparative atomic volumes and the nearest neighbor distances. At 77K the compounds are ferromagnetic. The Fe atoms exhibit different magnetic moments on the four sites. The decrease in Curie temperature and magnetization of Y_6Fe_{23} with increasing Al content arises as a result of two effects, dilution of the Fe sublattice with nonmagnetic atoms and changes in the preferential atomic ordering which govern the local environments of the Fe atoms so as to decrease the average Fe moment.

The ternary alloys, $Y_6(Fe_xMn_{1-x})_{23}$, exhibit interesting magnetic behavior over a range of solid solutions of iron and manganese. The transition metal atoms occupy four crystallographically different sites. For x less than ca. 0.27, the transition metal atoms couple ferromagnetically, whereas for greater values of x they couple antiferromagnetically. By using the iron populations for each site, obtained from neutron diffraction studies, it is possible to determine the Mossbauer effect hyperfine parameter fields for each site. As x increases, the ordering temperature decreases dramatically. At 1.3K in Y_6Fe_{23}, the four hyperfine fields range from 372koe to 250kOe, whereas in $Y_6(Fe_{0.52}Mn_{0.48})_{23}$ they decrease to values between 100kOe and 10kOe. This decrease apparently results from the increasing frustration of the ferromagnetic iron-iron coupling as additional manganese, which would prefer antiferromagnetic coupling, is introduced into the alloys.

The effects of the substitution of Fe by Al in $R_2(Fe_{1-x}Al_x)_{14}B$ compounds (R = Y, rare earths) on their magnetic properties have been investigated. The compounds crystallize in the tetragonal structure, $P4_2/mnm$, provided x < 0.1. The saturation magnetization and Curie temperatures decrease slightly with increasing Al content, x. However, the anisotropy constant, K_1, and the anisotropy field, H_A, exhibit a maximum at x = 0.06. The substitution of Fe with Al atoms is also effective in enhancing the coercivity of magnets based on the Nd-Fe-B compounds. As the Y atom carries no magnetic moment, the increased anisotropy field must result from preferential ordering of the non-magnetic Al atoms among the six non-equivalent crystallographic sites of the iron sublattice. Earlier work has shown that the replacement of Fe by Co results in increasing the Curie temperature and decreasing the coercive field. The present experimental data indicate that intermetallic compounds based on $Nd_2(Fe_{1-x-y}Al_xCo_y)_{14}B$ have both high Curie temperatures and high coercive fields. Accordingly, it appears that it is possible to improve the thermal properties and reduce the total losses of Nd-Fe-B magnets by appropriate substitution of Fe with Al and Co atoms. A spin reorientation appears at 140 K in $Nd_2Fe_{14}B$. In order to investigate the magnetic behavior of the rare earth sublattice, the magnetocrystalline anisotropy of $(Nd_{1-x}Sm_x)_2Fe_{14}B$ and $(Nd_{1-x}Pr_x)_2Fe_{14}B$ has been studied by X-ray and magnetic measurements. We find that the substitution of Nd with Sm results in an increasing spin reorientation temperature. A change in easy magnetization direction from the c-axis toward the basal plane is observed at room temperature in $(Nd_{1-x}Sm_x)_2Fe_{14}B$ compounds by increasing the

Sm content, x. The effect of substitution of Nd with Pr is reversed.

Accesion For	
NTIS CRA&I	☑
DTIC TAB	☐
Unannounced	☐
Justification	
By	
Distribution /	
Availability Codes	
Dist	Avail and/or Special
A-1	

TABLE OF CONTENTS

LIST OF ILLUSTRATIONS

LIST OF TABLES

I. MAGNETIC STRUCTURE OF Ho_6Mn_{23}

A. <u>INTRODUCTION</u>

Ho_6Mn_{23} crystallizes in the cubic Th_6Mn_{23} type structure. This structure consists of five non-equivalent lattice sites. The Ho occupies a single lattice site, e. Manganese occupies four lattice sites, b, d, f_1, and f_2. In this structure the local site symmetry of the Ho atom is not cubic, but uniaxial with point symmetry 4mm. The major axis is along <111>. For uniaxial symmetry the anisotropy is governed by the second order term in the crystal field Hamiltonian. The sign of the second order Stevens coefficient for the atom defines the easy direction of magnetization for the atom, a positive sign indicating an easy direction parallel to the uniaxis and a negative sign indicating an easy plane perpendicular to the uniaxis. For Dy and Ho the second order Stevens coefficient is negative, indicating that the easy direction of magnetization for Ho_6Mn_{23} and Dy_6Mn_{23} should be <110>. The magnetization measurements performed by Hardman et.al. on a single crystal of Dy_6Mn_{23} [1,2] do show this to be true for the Dy compound. However, the magnetization versus internal magnetic field curves for the three directions [110], [111] and [100] at 4.2K show that at this temperature the saturation magnetization is not reached even for extremely high fields (100-150 kOe). This indicates a non-collinear magnetic structure for the compound. Although a similar single crystal experiment has not been performed on Ho_6Mn_{23} thus far, since both Dy and Ho have negative second order Stevens coefficients in their crystal Hamiltonian and since they both crystallize in the same crystal structure, a similar non-collinear magnetic structure would be expected for Ho_6Mn_{23} as well. Magnetization measurements performed on polycrystalline

1

samples of Ho_6Mn_{23} by Pourarian et.al. [3] show that the saturation magnetization decreases very rapidly with temperature. At 4.2K the magnetization of the sample at a magnetic field of 50 kOe is found to be $59.8\mu_B$/f.u., whereas at 77K the magnetization approaches approximately $36\mu_B$/f.u. (figure 1). This could possibly indicate an increasing magnetic disorder in the rare earth sublattice, leading to a lower average magnetic moment per atom.

B. EXPERIMENTAL

Ho_6Mn_{23} was prepared by melting together stoichiometric amounts of Ho and Mn (>99.9% purity) in a water-cooled copper boat, using rf induction heating in an atmosphere of gettered argon. The alloy ingot was turned over and melted several times to assure sample homogeneity. A powder x-ray diffraction pattern of the cast Ho_6Mn_{23} was recorded on a GE diffractometer using CuKS radiation. The diffraction pattern showed only peaks belonging to a single phase.

High-resolution neutron diffraction measurements were made on the powdered sample contained in a cylindrical vanadium can at the University of Missouri Research Reactor facility in Columbia. The patterns from $2\theta=6.5^\circ$ to 80° were measured using a five detector powder unit at a wavelength of 1.293+. The data were analyzed using a modified Rietveld profile refinement procedure which includes fitted background parameters. The magnetic form factor for Ho was that measured by Koehler et.al. [4], and that for Mn was taken from Shull and Wollan [5]. Nuclear scattering amplitudes of Ho (equal to 0.850×10^{-12} cm) and Mn (-0.370×10^{-12} cm) were obtained from Bacon [6].

C. RESULTS AND DISCUSSION

The refined structural parameters for Ho_6Mn_{23} at 77K in the Fm3m structure are given in Table I. No constraints were used in the final refinement. the value of χ, defined as the ratio of the R-factor of the
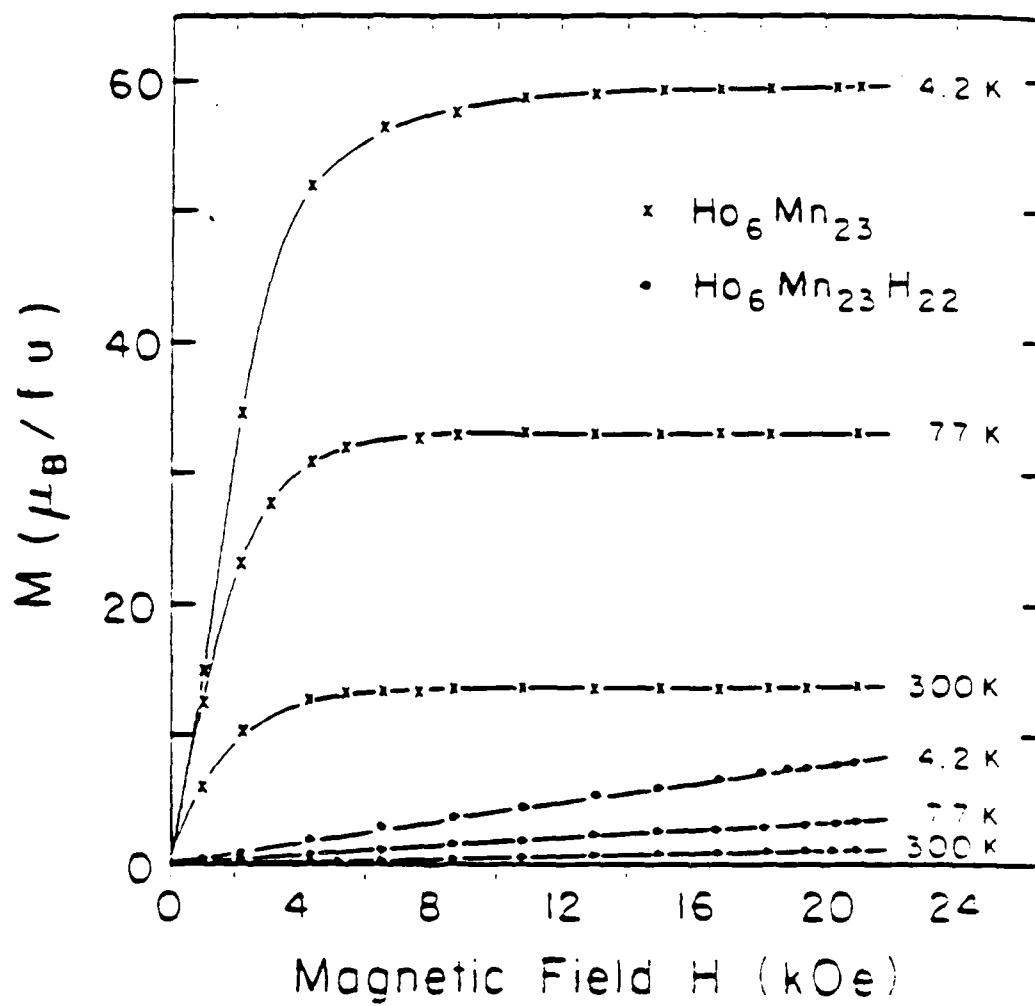
Figure 1. Magnetization curves for $Ho_6Mn_{23}D_{22}$ at 300K, 77K, and 4.2K.

TABLE I

REFINED ATOMIC PARAMETERS FOR Ho_6Mn_{23} AT 77K IN THE
Fm3m STRUCTURE

Site	Refined coordinates			Population
	x	y	z	
Ho e	0.2043	0.0	0.0	0.1496
Mn b	0.5	0.5	0.5	0.025
Mn d	0.0	0.25	0.25	0.1500
Mn f_1	0.1775	0.1775	0.1775	0.2000
Mn f_2	0.3791	0.3791	0.3791	0.2000

Cell parameter,a $= 12.3282 \pm 0.004A$

Temperature factor for Ho $= 0.0$

Temperature factor for Mn $= 0.0$

R-factor (weighted profile) $= 3.31\%$

R-factor (expected) $= 1.55\%$

X $= 2.14$

R-factor (nuclear) $= 5.64\%$

Computer refined stoichiometry for the compound is
$Ho_6Mn_{23.06}$

weighted profile to the expected R-factor, gives an indication of the quality of the fit. Since the expected R factor for our data is very low (1.55%), a value for χ of 2.14 is acceptable. The neutron diffraction scan for Ho_6Mn_{23} is shown in figure 2. The dotted profile represents the actual data points, and the smooth curve represents the calculated values.

The isotropic temperature factor and the B-factors (individual thermal factors) for the individual atoms were constrained to be zero. When these constraints were lifted, the thermal factors tended to be slightly negative (approximately -0.01 for Ho and -0.1 for Mn). Since negative thermal factors are unphysical, they were arbitrarily set equal to zero. The temperature factor, scale factor and background have high correlation coefficients in the Rietveld method. Accordingly, the negative temperature factors probably result from errors generated elsewhere in the fitting routine, and which accumulate in the temperature factors in an attempt to minimize the overall R-factor.

The cell parameters and the relative atom positions of Ho_6Mn_{23} were compared with those of Ho_6Fe_{23}, Y_6Mn_{23} and Y_6Mn_{23} in order to detect any systematic trends (Table II). All four compounds are believed to crystallize in the Fm3m, Th_6Mn_{23}, structure.

For a given rare earth atom R, there is a large difference in the cell parameter between the R_6Mn_{23} and the R_6Fe_{23} compounds. When R is Dy, Ho, Er, or Tm this difference is about 0.3A. For Lu the difference in cell size is approximately 0.26A, and for Y it is 0.37A. Thus, the difference in cell size seems to arise mainly from the relative sizes of the Mn and Fe atoms. Mn atoms, being the larger, are contained in a crystal structure with a larger unit cell. The variation among the rare earth systems may be due to the difference in size of the rare earth atoms and differences in bonding.

5
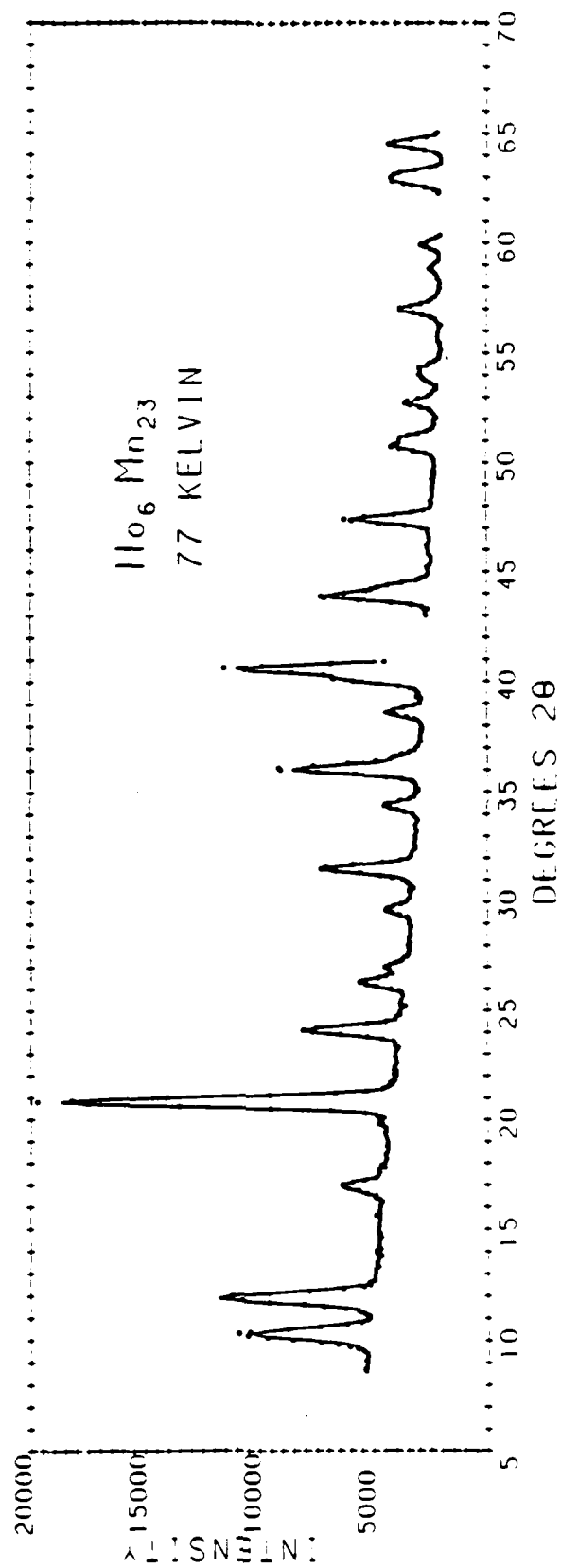
Figure 2. Data and refined neutron diffraction pattern for Ho_6Mn_{23} at 77K.

$Ho_6 Mn_{23}$

77 KELVIN

DEGREES 2θ

INTENSITY

6

TABLE II

A COMPARISON OF ATOMIC PARAMETERS OF THE Th_6Mn_{23} TYPE STRUCTURES

Compound	Temp	a_o	$e(x)$	$f_1(x)$	$f_2(x)$
Ho_6Mn_{23}	78K	12.328	0.2043	0.1775	0.379
Ho_6Fe_{23}	78K	12.004	0.205	0.175	0.379
Y_6Mn_{23}	4K	12.403	0.205	0.179	0.379
Y_6Fe_{23}	300K	12.063	0.207	0.177	0.379

A comparison of the atom positions in Ho_6Mn_{23}, Ho_6Fe_{23}, Y_6Mn_{23} and Y_6Fe_{23} (Table II) shows that in all four systems the relative positions of all the 98 atoms remain essentially the same. There is a very slight variation in the position of the f_1 site. In both Ho and Y systems the position of the f_1 site is slighty shifted (x increases by $0.002a_o$ when the transition metal is changed from Fe to Mn.) However the change is so slight that it is difficult to draw any conclusions from it. If this shift is real, then it is due to the changes in transition metal-transition metal interactions. It is not influenced by any rare earth interactions.

The refined magnetic moments for Ho_6Mn_{23} are given in Table III. The best refined structure proved to be non-collinear, with the Ho moments at an angle of 33° to the Mn moments. Since the structure is cubic, it is not possible to obtain the absolute moment directions from the Rietveld refinement programs. It has previously been established [7], using polarized neutron and magnetization data, that in Y_6Mn_{23} the Mn moments align ferrimagnetically along the body diagonal (the <111> direction). In Ho_6Mn_{23} the moments are also aligned ferrimagnetically. The b and d moments are antiparallel to the f_1 and f_2 moments. It is reasonable to believe that these moments lie along the <111> axis, or close to it. A comparison of the 100 Mn moments in Ho_6Mn_{23} with those in Y_6Mn_{23} are given in Table IV.

Both neutron diffraction [7] and polarized neutron beam [8] experiments have been previously performed on Y_6Mn_{23} at 4K and 295K. The value of the Mn moment at 77K should be closer to that obtained at 4K than that obtained at 295K. There is a fairly wide variation in the reported data. Our values of 2.0, 2.2 and $1.9\mu_B/f.u.$ for the Mn moments at the d, f_1 and f_2 sites respectively agree fairly well with the equivalent moments for Y_6Mn_{23} at 4K. The moment of $2.1\mu_B/f.u.$ at the b site is somewhat lower than expected.

8

TABLE III

MAGNETIC MOMENTS IN μ_B/ATOM FOR Ho_6Mn_{23} AT 77K

Atom	Site	Moment		θ^a
Ho	e	3.8	± 0.1	33.4°
Mn	b	-2.1	± 0.3	0.0°
Mn	d	-2.01	± 0.06	0.0°
Mn	f_1	2.2	± 0.1	0.0°
Mn	f_2	1.85	± 0.07	0.0°

[a] Angle between the magnetic moment and the <111> direction of the unit cell.

Calculated bulk magnetic moment per f.u = 39.3μ_B

Experimental bulk magnetic moment per f.u = 36.0μ_B

Magnetic R-factor = 6.80%

TABLE IV

A COMPARISON OF MAGNETIC MOMENTS IN THE HOLMIUM AND YTTRIUM SYSTEMS

Compound	Temp(K)	Magnetic Moment (μ_B/f.u.)					T_c(K)
		R	M(b)	M(d)	M(f_1)	M(f_2)	
Ho_6Mn_{23}	77	3.83	-2.1	-2.0	2.2	1.9	434
Ho_6Fe_{23}	78	-9.3	2.2	1.1	1.5	1.9	510
Y_6Fe_{23}	77	0.0	3.22	1.34	1.54	1.62	484
.	4	0.0	2.14	1.90	2.11	2.32	
Y_6Mn_{23}	4	0.0	-3.05	-2.34	1.99	1.80	486
			-4.34	-2.85	2.08	2.17	
	295	0.0	-2.71	-1.97	1.61	1.43	
Polarized neutron data							
Y_6Mn_{23}	4.2	0.0	-2.8	-2.07	1.79	1.77	
	300	0.0	-2.75	-1.72	1.52	1.27	

However, since the b site has a multiplicity of one compared with multiplicities for the d, f_1 and f_2 sites of 6, 8 and 8 respectively, the moment at the b site may carry a larger error. There is some doubt as to the validity of the magnitude of the errors for magnetic moments that are calculated by the Rietveld method [9]. Several authors have suggested that the actual errors in the moments may be much larger than those calculated by this method. However, to date a better method for calculation of the errors has not been found.

Due to the large asymmetry of the Ho 4f charge distribution, its moment should prefer to align in a plane perpendicular to the <111> direction. Quantitatively, this anisotropy can be given in terms of the Stevens coefficients. Although the crystal structure of Ho_6Mn_{23} is face centred cubic, the point symmetry of the Ho atom site is uniaxial, with the major axis being the cube axis on which the Ho atom lies. Thus, the second order terms of the crystal field are dominant. In terms of the Steven's formulation, the crystal field Hamiltonian of a Ho atom is

$$H = S\mu_B H_{ex} + S_J V_2^0 O_2^0.$$

V_2^0 is characteristic of the Ho atom environment, and the term $S_J V_2^0$ determines the strength of the anisotropy. For Ho, S_J is negative, indicating a planar anisotropy perpendicular to the uniaxis. On the other hand, the Mn moments in the absence of any other moments would align along the <111> direction. The angle between the actual Ho and Mn moments is 33°, suggesting that all the moments lie between the <110> and <111> directions, the Ho moment being close to the <110> direction and the Mn moment being closer to the <111> direction. It is expected that the Ho anisotropy is the dominant effect.

As determined from the neutron diffraction results, the Ho moment ($3.8\mu_B$/atom) is far removed from the free ion value of $10.6\mu_B$/atom.

Refinements in which large moments were forced on the Ho atom yielded very high R-values.

Except in the case of $HoFe_4Al_8$ [10], where no Ho moment was detected even at 4.2K, such a low value for the Ho moment has not been reported for any Ho-transition metal alloy at this temperature. For the cubic Laves phase structure of $HoMn_2$, the Ho moment at 4K was calculated to be $7.2\mu_B$/atom by Chamberlain [11], and $8.1\mu_B$/atom by Hardman et.al. [12]. Chamberlain suggested that the low Ho moment was due to a covalent moment transfer from Mn to Ho, making the net Ho moment lower. Hardman's results show a very low moment for the Mn atom ($-0.84\mu_B$/atom), which strengthens this argument. In Ho_6Mn_{23} all the Mn moments were found to be around $2\mu_B$/atom. Thus, even if there is such a covalent moment transfer, it should not lead to a very large reduction in the rare earth moment.

Since the lattice parameter and the atom positions are the same in Y_6Mn_{23} and Ho_6Mn_{23}, in the absence of rare earth-transition metal moment density interactions, the Mn atoms in Ho_6Mn_{23} should carry the same moments as those in Y_6Mn_{23}. If we take these to be 3.05, 2.34, -1.99 and $-1.84\mu_B$ at the b, d, f_1, and f_2 sites respectively, and compare with those obtained for Ho_6Mn_{23} of 2.1, 2.0, -2.2 and -1.9 μ_B/atom, then it is possible that there is moment transfer from the b and d sites. Taking multiplicities into account, this would reduce the Ho moment by about $0.5\mu_B$/atom. Thus Chamberlain's idea of covalent moment transfer from the Mn to the Ho atoms cannot account for the large reduction in the Ho moment.

Specific heat measurements were performed on Ho_6Mn_{23} by Tompson et.al. [13] in order to detect evidence for changes in the magnetic spin structure at low temperatures. The curve of specific heat against temperature did not show

a prominent peak which would indicate a structural change. The curves show an upward turn in the vicinity of 2K, the reason for which is not clear.

Thus, we can estimate a value for the Ho moment at 4K by using the bulk magnetic moment and the Mn moments obtained by neutron diffraction. If we assume that the angle between the Ho moment and the net Mn moment remains unchanged at 33.4° and that the Mn moments do not change significantly at the lower temperature, then to obtain a net magnetic moment of 59.8 μ_B/f.u. the Ho moment has to be approximately 7.3 μ_B/atom. This value is still significantly reduced from the free ion value of $10.6\mu_B$. The value of $7.3\mu_B$/atom gives an upper limit for the Ho moment at 4K. As the temperature is reduced from 77K to 4K, it is possible that the angle between the moments of the two sublattices decreases also. This would further reduce the Ho moment.

The low moment on the Ho atoms may stem from disorder in the Ho sublattice. Ho atoms are bound to each other by indirect coupling. These are by far the weakest type of coupling in the lattice. 3d-3d couplings and rare earth-3d couplings rule the lattice, and the R moments arrange according to this. The R moments are regarded as trivalent localized moments (R^{3+}). Since the spatial extent of the 4f wavefunctions is small, this assumption is justified in many cases. Since the 4f wavefunctions do not overlap, the presence of exchange interactions is explained as due to indirect exchange via spin polarization of the s conduction electrons. This type of interaction is known as Rudermann-Kittel-Kasuya-Yosida (RKKY)type. The weakly coupled rare earth moments may be fanning around the net Ho moment direction. This would lead to a reduction in the spatially averaged moment. Such spatial averaging has been suggested for $HoFe_2D_{3.5}$ by Rhyne et.al. [14]. As the temperature is increased from 4K to 77K the disorder would increase, further lowering the moment. The fact that the Ho moment is high in Ho_6Fe_{23} may be

explained as being due to a smaller unit cell size. The Ho-Fe interaction may be stronger than the Ho-Mn interaction due to the smaller interatomic distance. The zero Ho moment in $Ho_6Fe_4Al_8$ may be due to its extremely low ordering temperature (25±5K) which corresponds to the onset of long range order in the transition metal sublattice. Since the rare earth-3d interactions are an order of magnitude weaker than the 3d-3d interactions, a temperature of 4.2K may not be sufficiently low for the rare earth sublattice to order.

The experimental bulk magnetic moment at 77K has been found to be approximately $36\mu_B$/f.u. by Pourarian et.al. [3]. The calculated value from our neutron diffraction results is $39.6\mu_B$/f.u. The value calculated from the neutron data is not very reliable because of the large overall error which is produced when summing the individual moments of the 29 atoms in the unit cell.

II. MAGNETIC AND CRYSTALLOGRAPHIC STRUCTURE OF $Ho_6Mn_{23}D_{22}$

A. INTRODUCTION

Ho_6Mn_{23} falls into the category of a large class of compounds having the general formula R_6M_{23}, where R is a rare earth or actinide and M is Fe or Mn. The crystal structures of these compounds are face-centered cubic, space group Fm3m. There are four formula units per unit cell. The rare earth atom occupies a unique e site which has a uniaxial point symmetry, while the transition metal atoms occupy the b, d, f_1, and f_2 sites.

Most of these compounds have very interesting and unusual magnetic properties. When H or D atoms are introduced into these compounds, the magnetic properties often change dramatically. For example, Y_6Mn_{23} is a ferrimagnet with a Curie temperature of 486K, while its hydride is a Pauli paramagnet. In contrast, the isostructural compound Th_6Mn_{23} is a Pauli paramagnet at room temperature, but becomes ferrimagnetic upon the introduction of H atoms into the system.

Neutron diffraction studies performed on $Y_6Mn_{23}D_{23}$ [15], $Th_6Mn_{23}D_{16}$ [16], and $Ho_6Fe_{23}D_x$ (x = 1.5, 8.2, 15.7) [7] show that these compounds retain the face-centered cubic structure of the parent compound at room temperature, but transform to a tetragonal structure (space group P4/mmm) below the magnetic ordering temperature. The exceptions are $Th_6Mn_{23}D_{30}$ [16], which retains the Fm3m structure down to 4K, and $Ho_6Fe_{23}D_{12.1}$ [17], which has has been analyzed assuming a body-centered tetragonal structure, space group I4/mmm, at room temperature.

Structural analysis of $Y_6Mn_{23}D_{23}$ at 78K and 4K reveals that the moments on the Mn atoms order themselves to yield a weakly antiferromagnetic structure. The Mn moments that are ordered lie along the uniaxial direction of the tetragonal cell. In contrast, the Ho and Fe moments in $Ho_6Fe_{23}D_x$ compounds lie in the basal plane. Thus, in Ho_6Mn_{23} and its deuterides there are two opposing effects of anisotropy, the Mn atoms which tend to align moments out of the basal plane and the Ho atoms which favor the moments to lie in the basal plane.

The non-deuterated Ho_6Mn_{23} compound has a Curie temperature of 434K, and a bulk magnetic moment of approximately 36 μ_B mol^{-1} at 77K and 59.3 μ_B mol^{-1} at 4.2K. It crystallizes in the Th_6Mn_{23}-type, face-centered cubic structure. At 77K its magnetic structure is non-collinear with the Ho moments tilted at an angle of 33.4° to the Mn moments. The Ho atom carries a moment of 3.3 μ_B while the Mn moments at the b, d f_1 and f_2 sites are 2.1, 2.0, 2.2 and 1.9 μ_B /atom respectively. Upon deuteration, the compound becomes antiferromagnetic, with a Neel temperature of approximately 100K.

Many studies have focussed on understanding the stability criteria and factors governing the hydrogen site preferences and the observed stoichiometries of intermetallic hydrides. The model put forward by Miedema and coworkers [18] relates the stabilities of the intermetallic hydrides to their enthalpy of formation. This model was extended by Jacob et.al. [19,20] to calculate enthalpies of formation of imaginary binary hydrides at the interstitial sites to determine the preferred sites for H or D occupation. This semiempirical model has been applied to some RM_2 and R_6Mn_{23} hydrides. Westlake [21-25] uses criteria of minimum hole size and minimum H-H distance to rationalize the observed H occupancies and stoichiometries of several types

of intermetallic hydrides. This geometric model has been successfully applied to several R_6Mn_{23} hydrides.

We have carried out powder neutron diffraction studies of $Ho_6Mn_{23}D_{22}$ at room temperature and 9K to determine its crystallographic structure, the distribution of the D atoms among the occupied sites, and the nature of the magnetic structure below the ordering temperature.

B. EXPERIMENTAL

An ingot of Ho_6Mn_{23} was prepared by induction melting of the 99.9% pure elements in the appropriate stoichiometric amounts in a water-cooled copper boat under an argon atmosphere. X-ray diffraction patterns exhibited only lines belonging to the face-centered cubic (Fm3m) single phase. The ingot was deuterated with 99.5% deuterium in a stainless steel vessel at 20 atm and $110^{\circ}C$ for 2 hours [26]. Pressure-volume measurements indicated approximately 23 atoms of deuterium absorbed per formula unit of Ho_6Mn_{23}. The deuteration shattered the ingot into a very fine powder which was then placed in an aluminum container for the diffraction experiments. Neutron diffraction data at room temperature and 9K were collected from $2\theta5^{\circ}$ to 80° at 0.1° intervals using a two-axis diffractometer at the University of Missouri Research Reactor at Columbia ($\lambda=1.293A$). The data were analyzed using a modified Rietveld profile technique [27]. In the final refinement no constraints were used. The deuterium populations at the different sites and the magnetic moments on the Ho and Mn atoms could not be refined at the same time due to large correlation coefficients which produced unrealistic values for these parameters. They were refined alternately until the R factors and χ values were minimized. The scattering lengths for Ho, Mn and D were obtained from Bacon [6]

$$b_{Ho} = 0.850 \times 10^{-12} \text{ cm}$$

$$b_{Mn} = -0.370 \times 10^{-12} \text{ cm}$$

$$b_D = 0.667 \times 10^{-12} \text{ cm.}$$

C. RESULTS AND DISCUSSION

1. <u>Crystallographic structure of $Ho_6Mn_{23}D_{22}$ at 298 and 9K.</u> At 298K, $Ho_6Mn_{23}D_{22}$ has no long range magnetic ordering, whereas at 9K it is antiferromagnetically ordered. A comparison of the neutron diffraction spectra at the two temperatures shows that at the lower temperature additional peaks appear. To index these peaks it is neccessary to assume that that the compound has tetragonal symmetry at 9K. Since the non-deuterated compound Ho_6Mn_{23} is face-centered cubic, one is faced with the question of whether the structural transformation occurs upon deuteration, or only at the onset of magnetic order. Earlier neutron diffraction studies on $Y_6Mn_{23}D_{23}$ [26] and $Er_6mn_{23}D_{23}$ [28] were performed on the former assumption, and the structures both above and below the ordering temperatures were refined using a tetragonal body-centered unit cell, space group $I4/mmm$. A more recent study on $Y_6Mn_{23}D_{23}$ [15] using higher resolution data over a wider angular range ($2\theta = 10^{\circ}$ to 115°) shows that above the ordering temperature the peaks can be fitted using the $Fm3m$ space group and that there is no broadening or splitting of peaks relative to those of Y_6Mn_{23}. Thus, at room temperature the deuterated compound retains the face centered cubic structure of the parent compound. The high temperature scan of $Ho_6Mn_{23}D_{22}$ was fitted to both a $Fm3m$ structure and an $I4/mmm$ structure. The structural parameters are given in tables V and VI. In both cases the χ values are acceptable. The lower χ value in the $I4/mmm$ structure could arise from the lower symmetry of this structure when compared to that of the $Fm3m$ structure, which leads to more refinable parameters.

18

TABLE V

ATOMIC PARAMETERS FOR $Ho_6Mn_{23}D_{22}$ AT 298K IN THE FCC (Fm3m) STRUCTURE

Site	N	N(max)	Refined Coordinates x	y	z	B
Ho e	12	12	0.2054	0.0	0.0	0.23
Mn b	2	2	0.5	0.5	0.5	0.25
Mn d	12	12	0.0	0.25	0.25	0.25
Mn f_1	16	16	0.1803	0.1803	0.1803	0.25
Mn f_2	16	16	0.3701	0.3701	0.3701	0.25
D a	2	2	0.0	0.0	0.0	2.67
D f_3	11	16	0.0967	0.0967	0.0967	2.67
D j_1	18	48	0.0	0.1696	0.3700	2.67
D k	12	48	0.1623	0.1623	0.0464	2.67

Cell Parameter	a =	12.773 ± .001 A
R-factor (weighted profile)	=	4.83%
R-factor (expected)	=	2.45%
X	=	1.97%

Note: N is the refined occupancy of the site per two
       formula units
N(max) is the maximum occupancy
B is the Debye-Waller temperature factor.

TABLE VI

STRUCTURAL PARAMETERS FOR $Ho_6Mn_{23}D_{22}$ IN THE $I4/mmm$ SPACE GROUP

Site	Refined Coordinates x	y	z	Population N	B
Ho e	0.0	0.0	0.205	0.05	0.47
Ho h	0.205	0.205	0.0	0.10	0.47
Mn b	0.0	0.0	0.5	0.025	0.42
f	0.25	0.25	0.25	0.10	0.42
c	0.50	0.0	0.0	0.05	0.42
n_1	0.360	0.0	0.180	0.20	0.42
n_2	0.743	0.0	0.372	0.20	0.42
D a	0.0	0.0	0.0	0.024	3.61
n_3	0.203	0.0	0.093	0.147	3.61
l^3	0.561	0.170	0.0	0.059	3.61
m	0.368	0.368	0.156	0.159	3.61
o	0.208	0.118	0.166	0.124	3.61

$a = 9.004 \pm 0.004 A$
$c = 12.641 \pm 0.010 A$

R-factor (profile)   =3.3%
R-factor (weighted profile =4.17%
X   =1.74

At 9K, the compound has a tetragonal structure. Two possible space groups which fit this structure are I4/mmm and P4/mmm. Hardman et.al. [15] observed that the neutron diffraction pattern for $Y_6Mn_{23}D_{23}$ contained peaks at $2\theta=56.3^\circ$, 69.4° and 69.9° that were predominantly nuclear peaks, which are not allowed in the I4/mmm space group, but which are allowed in the P4/mmm space group. A careful inspection of the spectrum of $Ho_6Mn_{23}D_{22}$ showed that the peaks were not sufficiently resolved in this region to pick out similar individual reflections which would conclusively determine the correct space group. However, the Rietveld refinement gave a much better fit to the model having space group P4/mmm. The model assuming I4/mmm space group gave an especially poor fit at the peak at location $2\theta=42.5^\circ$. This peaks consists of two dominant contributions from the 226 and 432 reflections which are predominantly nuclear. The former reflection is allowed by both space groups, whereas the latter is only allowed in the P4/mmm space group. Thus, P4/mmm was chosen to be the correct space group representing the structure of $Ho_6Mn_{23}D_{22}$ at 9K. At room temperature the structure can be represented by the Fm3m space group, similar to that of $Y_6Mn_{23}D_{23}$. Figure 3 gives the profile fit to the neutron diffraction data assuming this structure.

At room temperature the deuterium atoms are found to occupy the a, f_3, j and k_1 sites. The number of atoms per formula unit at each of the sites is found to be 1, 5.5, 9 and 6 respectively. In $Y_6Mn_{23}D_{23}$ the deuterium atoms occupy the same sites with 1, 5, 10 and 7 atoms per formula unit respectively [15]. The structural parameters for $Y_6Mn_{23}D_{23}$ at 298K are given in Table VII. The relative atom positions for both atoms are essentially the same. The unit cell dimension in the Y compound is larger than that in the Ho compound. This could be due to either the lanthanide contraction which makes Ho a smaller atom than Y, or to differences in electronic effects between the Ho-Mn-D and
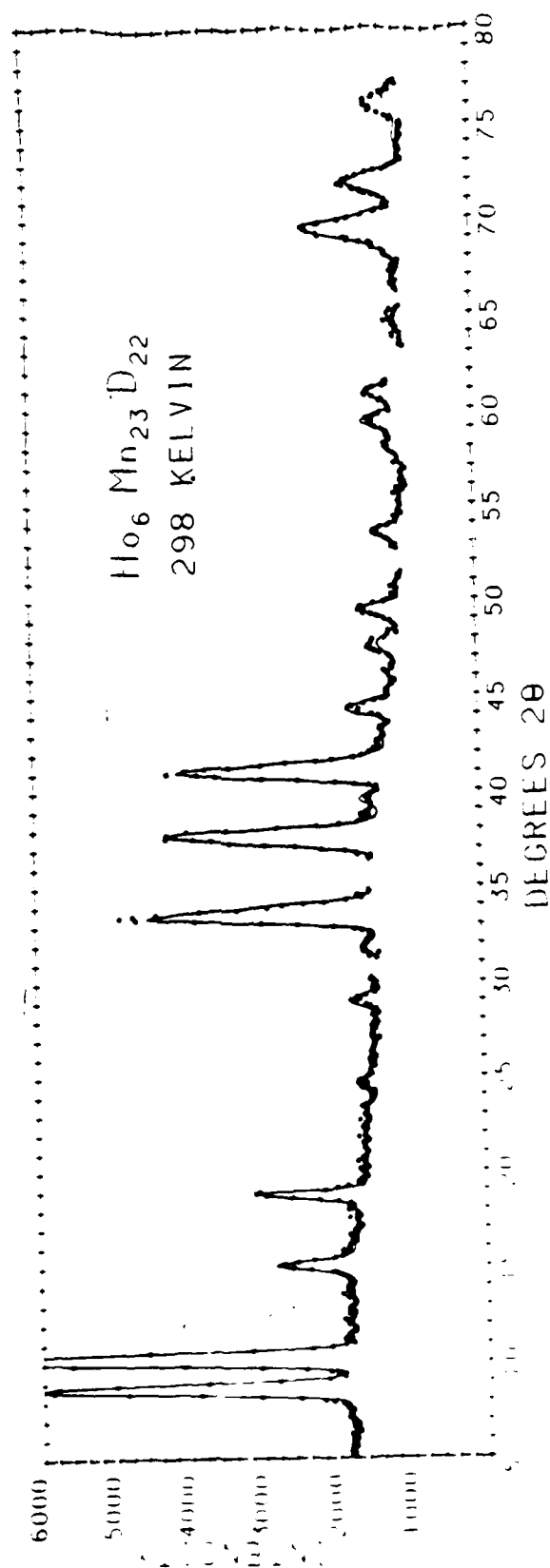
Figure 3. Data and refined neutron diffraction pattern for $Ho_6Mn_{23}D_{22}$ at 298K.

TABLE VII

ATOMIC PARAMETERS FOR $Y_6Mn_{23}D_{23}$ AT 298K IN THE FCC

(Fm3m) STRUCTURE

Site	N	N(max)	Refined Coordinates x	y	z	B
Y e	12	12	0.205	0.0	0.0	0.82
Mn b	2	2	0.5	0.5	0.5	0.47
Mn d	12	12	0.0	0.25	0.25	0.47
Mn f_1	16	16	0.179	0.179	0.179	0.47
Mn f_2	16	16	0.372	0.372	0.372	0.47
D a	2	2	0.0	0.0	0.0	6.35
D f_3	10	16	0.100	0.100	0.100	1.37
D j_1	20	48	0.0	0.169	0.373	4.95
D k	14	48	0.161	0.161	0.049	2.28

Cell Parameter, a = 12.805 A

Y-Mn-D. Oesterreicher [29] has pointed out that it is often not possible to distinguish between size and electronic effects as both vary in a similar fashion in the periodic table.

The deuterium atom population amongst the various sites obtained in this study can be compared with those predicted by Jacob's heat of formation model [20] and with Westlake's geometric model [23,24]. In the former model the stability of the hydrogen atom at a given site is estimated by calculating the heat of formation of the imaginary binary hydrides formed between the hydrogen atom and the host metal atoms forming the interstitial site. By adding these heats of formation, a value of $\Delta H'$ is assigned to each site. The hydrogen occupation amongst the various interstices is obtained using the Boltzmann distribution function and the $\Delta H'$ values for the interstices. For the R_6M_{23} system Jacob considered seven interstices for possible hydrogen or deuterium occupation; a, f_3, k, j_1, i, l_2 and e_2. The four interstices having the largest negative $\Delta H'$ values, given in the order of decreasing absolute magnitude, are a, f_3, k and i. A neutron diffraction study by Commandre et.al. [30] found deuterium atoms at the a, f_3 and j sites. To explain these results Jacob modified the theory to account for H-H repulsive forces where neccessary. Due to the proximity of the f_3 site, the k site cannot be filled while the f_3 site is full. The hydrogen atom at the f_3 site would cause a strong electrostatic repulsive force at the k site. Thus deuterium atoms would completely fill the a and f_3 sites, then they would fill the i site. The distorted octahedral i site predicted by Jacob is in very close proximity to the j site reported by Commandre et.al. [30]. Our results for $Ho_6Mn_{23}D_{22}$ show that the deuterium atoms occupy the a, f_3, j and k sites. The distorted octahedral i site at (0.36,0.14,0) as described by Jacob correlates with our j site at (0.0,0.17,0.37). Contrary to the prediction by Jacob that the f_3 site

24

would be full and the k site empty, we find that the f_3 site contains 5.5 atoms, whereas its maximum occupancy is 8 atoms, and the k site contains 6 atoms. Thus our results do not agree completely with Jacob's model. The shortcomings of Jacob's model have been discussed by Westlake in a review article on intermetallic hydrides [22]. Among other objections, he points out that the enthalpy of formation of the intermetallic hydride is ignored, and that the hydrogen atom distribution function is arbitrary. He concludes that the agreement between theory and experiment is accidental and has no physical basis.

According to Westlake's model, in stable intermetallic hydrides the hydrogen atoms only occupy sites which are large enough to accomodate spheres of radius 0.40A. Due to the H-H repulsive forces, there is a minimum H-H distance of 2.1A. When more than one type of site meets the requirement according to hole size, then the hydrogen atoms occupy sites which yield the densest hydrogen packing within the limits of the minimum H-H distance requirement. The larger holes tend to be filled first, but are not neccessarily completely filled in order to allow hydrogen to occupy other sites if this leads to a larger hydrogen atom density. Also, sites of apparently low priority may be filled if they play an essential role in the diffusion mechanism. This effect is observed in the RMn_2 compounds [25].

According to this model the deuterium atoms in $Ho_6Mn_{23}D_{22}$ may occupy the a, f_3, j_1 and k sites, which is in agreement with the present neutron diffraction results. Westlake also considered the i, j_2, h and l as possible sites for hydrogen or deuterium occupation. Our refinements do not show any deuterium atoms to be at any of these positions.

Westlake's model leads to certain restrictions on the occupation numbers of the D atom sites. The D atoms are predicted to fill the holes in the order

25

of decreasing hole size keeping all nearest neighbor D-D distances larger than 2.1A. Accordingly, all the octahedral a sites should be occupied first. These holes are very large and widely separated. They also have the largest number of rare earth neighbors. The second largest holes are the f_3 sites. If the f_3 sites are completely filled, then the next largest sites, k_1, must remain empty since the f_3-k_1 distances are only about 1.3A, far less than the required minimum of 2.1A. The k site can accommodate a maximum of 20 D atoms if the f_3 site is empty, and for every D atom removed from the f_3 site, 3 D atoms can be added to the k_1 site. Thus, our results of 6 atoms at the k_1 site, and 5.5 at the f_3 site are in agreement with these restraints. The j_1 and j_2 sites are nearly the same size. They both have one Ho nearest neighbor. If the j_2 sites are empty, then half of the j_1 sites may be filled at the same time, that is, 12 atoms/f.u. Our results show 9 atoms at this site.

The refined thermal factors for Ho, Mn and D are 0.23, 0.25 and 2.67 respectively. Since deuterium is a much lighter atom than either Ho or Mn, a larger b factor is expected for it. A large value for the b factor may mean a loosely bound atom or a large atomic volume at that site. Thus, theoretically, by refining the b factors for each site individually instead of assigning a mean value, one might expect to gather information concerning the different interstices. However, the temperature factors obtained from the refinements carry large errors. The R factors do not vary significantly by allowing individual temperature factors at the different sites. Since it is difficult to draw any conclusions from these values, all the deuterium atoms were assigned the same temperature factor.

The space group P4/mmm provided the best fit to the nuclear structure of $Ho_6Mn_{23}D_{22}$ at 9K. Neutron diffraction studies performed on $Y_6Mn_{23}D_{23}$ and $Th_6Mn_{23}D_{16}$ by Hardman et.al. [15,16] using a high resolution diffractometer

26

and over a scattering angular range of up to 110° showed that these compounds too remain fcc at room temperature. All the peaks could be indexed assuming the Fm3m space group, while no broadening or splitting of peaks were observed. However, below 78K both compounds underwent a structural transition from cubic to tetragonal, space group P4/mmm. Similarly, the space group P4/mmm provided the best fit to the nuclear structure of $Ho_6Mn_{23}D_{22}$ at 9K. The neutron diffraction scan for this compound at 9K is given in figure 4. The dotted profile represents the actual data points, and the smooth curve corresponds to the calculated fit assuming the P4/mmm space group.

The equivalent positions in the two crystallographic space groups Fm3m and P4/mmm, together with the atom positions at 298K are given in Table VIII and IX. The (x,y,z) position in the Fm3m structure is related to the (x',y',z') position in the P4/mmm structure by the conversion

$$x' = x + y$$

$$y' = x - y$$

$$z' = z$$

There are four formula units per unit cell $(z=4)$ in the Fm3m structure while for the P4/mmm structure there are two (figure 5). Table X gives the refined parameters at 9K. According to the Westlake model [23,24], only half of the original j_1 sites can be filled. Thus, the p and q sites in the tetragonal cell can only be half filled, while only two of the four r sites can be filled at the same time, or all four r sites may be only half filled. Our results show that the r_3 and r_5 sites are empty, whereas the r_2 and r_4 sites are filled. Both the p and q sites are less than half filled. Moderate shifts (approximately $0.04a_o$) in position from the fcc structure are observed for some sites. The populations at the s_4, t_4, and u_1 sites are quite small. Therefore, the error in the refined coordinates of these three positions may

27
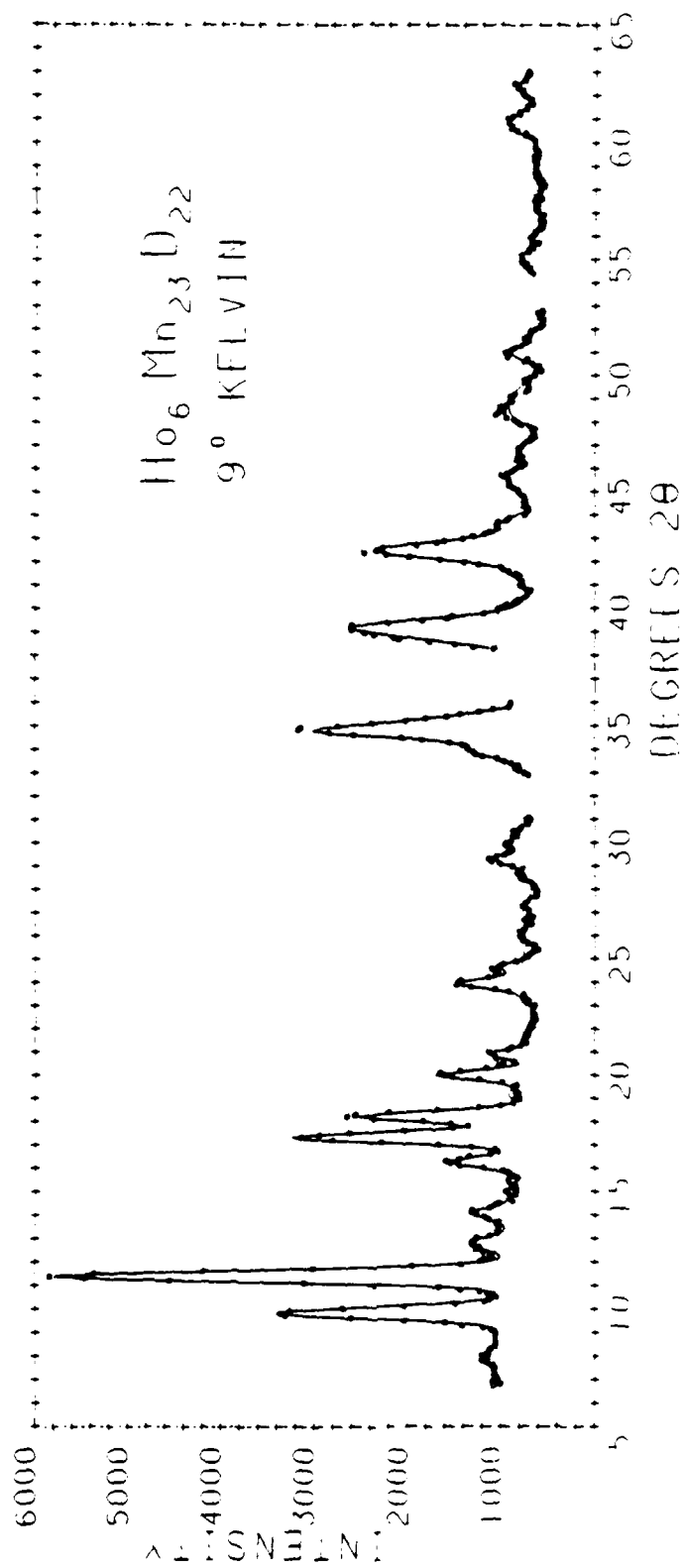
Figure 4. Data and refined neutron diffraction pattern for $Ho_6Mn_{23}D_{22}$ at 9K.

28

TABLE VIII

EQUIVALENT POSITIONS IN THE Fm3m AND P4/mmm SPACE GROUPS

Site(Fm3m)	N/2 per f.u	Site(P4/mmm)	N/2 per f.u.
Y $e(x,0,0)$	12	$g(0,0,z)$	2
		$h(0.5,0.5,z)$	2
		$j(x,x,0)$	4
		$k(x,x,0.5)$	4
Mn $b(0.5,0.5,0.5)$	2	$b(0,0,0.5)$	1
		$c(0.5,0.5,0)$	1
Mn $d(0,0.25,0.25)$	2	$e(0,0.5,0.5)$	2
		$f(0,0.5,0)$	2
		$r_1(x,x,z)$	8
Mn $f_1(x,x,x)$	16	$s_1(x,0,z)$	8
		$t_1^1(x,0.5,z)$	8
Mn $f_2(x,x,x)$	16	$s_2(x,0,z)$	8
		$t_2^2(x,0.5,z)$	8
D $a(0,0,0)$	2	$a(0,0,0)$	1
		$d(0.5,0.5,0.5)$	1
D $f_3(x,x,x)$	16	$s_3(x,0,z)$	8
		$t_3^3(x,0.5,z)$	8
D $j_1(0,y,z)$	48	$p(x,y,0)$	8
		$q(x,y,0.5)$	8
		$r_2(x,x,z)$	8
		$r_3(x,x,z)$	8
D		$r_4(x,x,z)$	8
		$r_5(x,x,z)$	8
D $k(x,x,z)$	48	$s_4(x,0,z)$	8
		$t_4(x,0.5,z)$	8
		$u_1(x,y,z)$	16
		$u_2(x,y,z)$	16

TABLE IX

ATOMIC PARAMETERS OF $Ho_6Mn_{23}D_{22}$ AT 298K TRANSFORMED

TO COORDINATES OF THE TETRAGONAL CELL (P4/mmm SITES)

Atom	Fm3m site	P4/mmm site	Refined Coordinates x	y	z
Ho	e	g	0.0	0.0	0.2054
		h	0.5	0.5	0.2946
		j	0.2054	0.2054	0.0
		k	0.2946	0.2946	0.5
Mn	b	b	0.0	0.0	0.0
		c	0.5	0.5	0.0
Mn	d	e	0.0	0.5	0.5
		f	0.0	0.5	0.0
		r_1	0.25	0.246	0.75
Mn	f_1	s_1	0.3606	0.0	0.1803
		t_1	0.1394	0.5	0.3197
Mn	f_2	s_2	0.2598	0.0	0.3701
		t_2	0.2402	0.5	0.1299
D	a	a	0.0	0.0	0.0
		d	0.5	0.5	0.5
D	f_3	s_3	0.1934	0.0	0.0967
		t_3	0.3066	0.5	0.4033
D	j	p	0.2044	0.4604	0.0
		q	0.2996	0.0396	0.5
		r_2	0.13	0.13	0.3304
		r_3	0.1696	0.1696	0.37
		r_4	0.3304	0.3304	0.13
		r_5	0.37	0.37	0.1696
D	k_1	s_4	0.3246	0.0	0.0464
		t_4	0.1754	0.5	0.4536
		u_1	0.1159	0.2087	0.1623
		u_2	0.2913	0.3848	0.3377
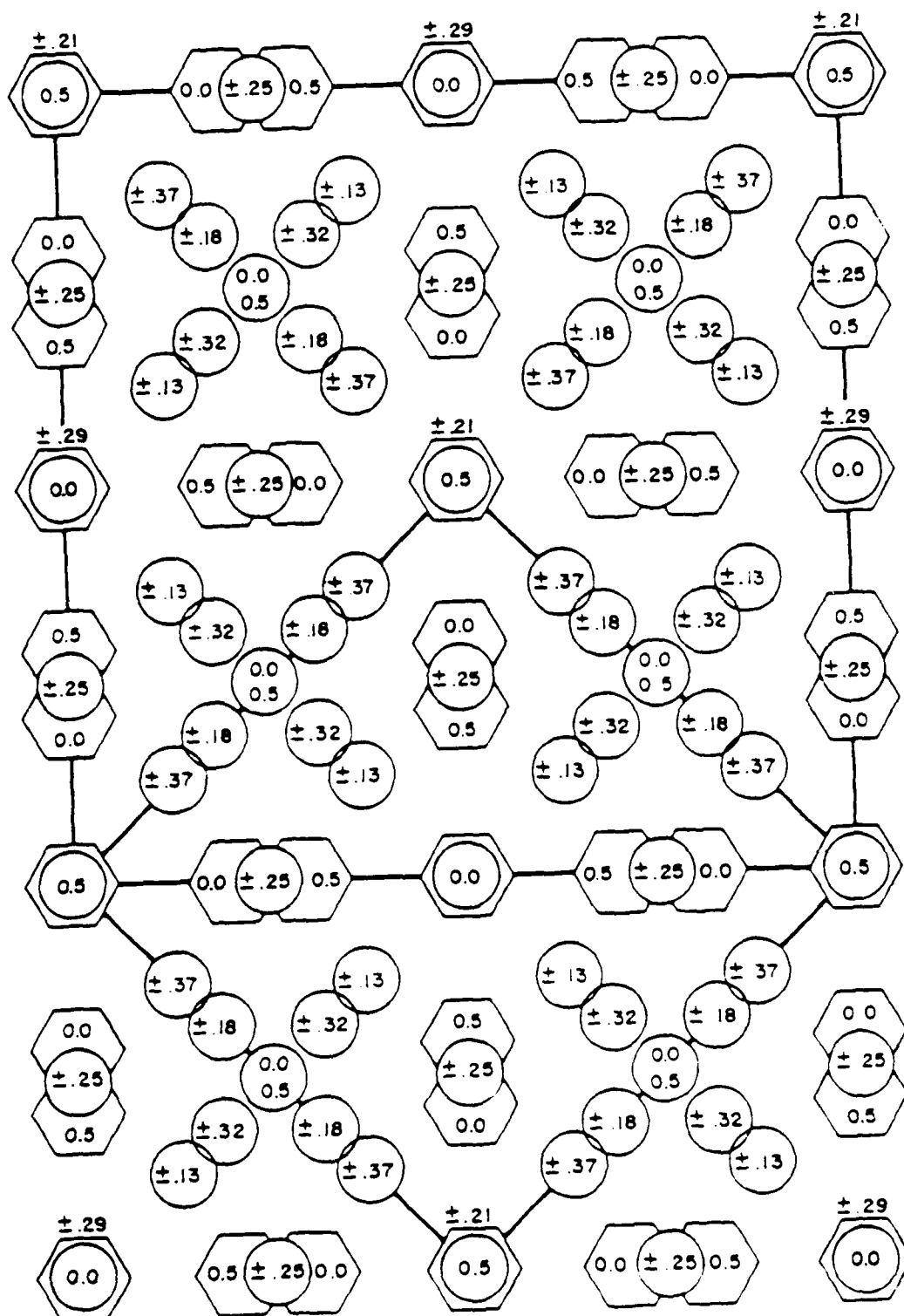
Figure 5. Cubic and tetragonal unit cells for the
Th₆Mn₂₃ structure.

TABLE X

ATOMIC PARAMETERS OF $Ho_6Mn_{23}D_{22}$ AT 9K IN THE P4/mmm

TETRAGONAL STRUCTURE

fcc sites	Tetragonal sites	N	Refined Coordinates x	y	z	B
Ho e	Ho g	2	0.0	0.0	0.201	0.01
	h	2	0.5	0.5	0.304	0.01
	j	4	0.222	0.222	0.0	0.01
	k	4	0.299	0.299	0.5	0.01
Mn b	Mn b	1	0.0	0.0	0.0	0.2
	c	1	0.5	0.5	0.0	0.2
Mn d	Mn e	2	0.0	0.5	0.5	0.2
	f	2	0.5	0.5	0.5	0.2
	r_1	8	0.246	0.246	0.762	0.2
Mn f_1	Mn s_1	8	0.329	0.0	0.161	0.2
	t_1	8	0.103	0.5	0.312	0.2
Mn f_2	Mn s_2	8	0.256	0.0	0.399	0.2
	t_2	8	0.266	0.5	0.150	0.2
D a	D a	1	0.0	0.0	0.0	0.42
	d	1	0.5	0.5	0.5	0.42
D f_3	D s_3	3.2	0.152	0.0	0.059	0.42
	t_3	8	0.270	0.5	0.387	0.42
D j	D p	3.2	0.191	0.449	0.0	0.42
	q	2.6	0.199	0.995	0.5	0.42
	r_2	8	0.144	0.144	0.326	0.42
	r_3	0	---	---	---	---
	r_4	4	0.335	0.335	0.059	0.42
	r_5	0	---	---	---	---
D k	D s_4	1.4	0.238	0.0	0.117	0.42
	t_4	1.4	0.192	0.5	0.458	0.42
	u_1	0.4	0.188	0.134	0.162	0.42
	u_2	8	0.277	0.380	0.322	0.42

TABLE X
(continued)

Cell Parameters	a	=	8.9814A
	c	=	12.6383A

R-factor (weighted profile)	=	5.71%
R-factor (expected)	=	3.02%
X	=	1.9
R-factor (nuclear)	=	5.73%

be quite large. The Ho j site has shifted relative to its position in the original cubic cell more than the other three Ho sites. The largest change in Mn positions occurs at the f_1 site. In the $Y_6Mn_{23}D_{23}$ compound the largest shift is at the f_2 site [15]. The lattice parameters of this cell are a=8.981A and c=12.638A. This gives a ratio $c/a\sqrt{2}$=0.995, which is an indication of the extent of the tetragonal distortion.

2. Magnetic structure of $Ho_6Mn_{23}D_{22}$ at 9K. Analysis of the data at 9K reveals a noncollinear antiferromagnetic structure with the Ho moments at the g and j sites coupled antiparallel to the h and k sites respectively. Table XI lists the refined moments. The moments of Ho_6Mn_{23} are also tabulated for comparison purposes (table XII). Surprisingly, the Ho moments on all four crystallographic positions are approximately 3.5 μ_B/atom, far removed from the free ion value ($gJ = 10$ μ_B for Ho^{3+}, usually obtained for Ho in metals). If the Ho moments are constrained to be about 10 μ_B/atom, the refinement becomes divergent. The direction of the Ho moments at the j and k sites lie very close to the basal plane, while those at the g and h sites are closer to the 101 direction. The 101 direction in the tetragonal cell corresponds to the 111 direction in the cubic cell. The values of the Mn moments at the b, c, s_2, and t_2 sites agree well with the values reported by Hardman-Rhyne et al [15] for $Y_6Mn_{23}D_{23}$ (see table XII), although the directions of the moments in $Ho_6Mn_{23}D_{23}$ are tilted away from the c axis. This is undoubtedly due to the anisotropy of Ho, which prefers to align its moments in the basal plane. No magnetic moments for Mn are observed at the e, f, s_1, and t_1 sites in the $Y_6Mn_{23}D_{23}$ compound, whereas in the deuterated Ho_6Mn_{23} compound these sites carry moments of 2.37, -2.37, -2.82, and 2.82 μ_B respectively (the sign indicates the direction of the magnetic moments). This difference is probably

TABLE XI

MAGNETIC MOMENTS FOR $Ho_6Mn_{23}D_{22}$ AT 9K

Site		Moment (μ_B/atom)	θ^a (degrees)
Ho	g	3.4	51.4
	h	3.4	128.6
	j	3.5	100.1
	k	3.5	.79.9
Mn	b	3.5	29.5
	c	3.5	150.5
	e	2.3	67.7
	f	2.3	112.3
	r_1	0	0
	s_1	2.8	117.5
	t_1	2.8	62.5
	s_2	1.5	30.3
	t_2	1.5	149.7

$^a\theta$ is the angle between the magnetic moment and the c axis.

Magnetic R-factor = 13.3%

TABLE XII

A COMPARISON OF MOMENTS IN Y_6Mn_{23} AND Ho_6Mn_{23}

COMPOUNDS AND THEIR HYDRIDES

	Ho_6Mn_{23}	Y_6Mn_{23}			$Ho_6Mn_{23}D_{22}$	$Y_6Mn_{23}D_{22}$
R e	3.8	0	R	g	3.4	0
				h	-3.4	0
				j	-3.5	0
				k	3.5	0
Mn b	-2.1	-3.05	Mn	b	3.5	-3.6
				c	-3.5	3.6
Mn d	-2.0	-2.34		e	2.3	0
				f	-2.3	0
				r_1	0	0
Mn f_1	2.2	1.99		s_1	-2.8	0
				t_1	2.8	2.08
Mn f_2	1.9	1.80		s_2	1.5	2.08
				t_2	-1.5	-2.08

36

due to the influence of the magnetic Ho atom neighbors which favors ordering of the Mn moments. Powder neutron diffraction studies performed on the non-deuterated Y_6Mn_{23} compound [8] indicate that the d and f_1 sites, which split into e and f, s_1 and t_1 sites, respectively, in the tetragonal system, carry moments of 2.85 and 2.08 μ_B (see table XII). Polarized neutron diffraction studies [7] on the same compound yield values of 2.07 and 1.79 μ_B for these two sites. Our values of 2.37 and 2.82 μ_B are comparable to the results of these two studies.

There have been previous reports of Ho-transition metal compounds and their deuterides, where fairly low values have been observed for the Ho moments. Neutron diffraction measurements have been made on the cubic Laves phase compounds $HoMn_2$ and Ho(MnFe) by Chamberlain [11]. In $HoMn_2$, Ho was found to carry a moment of 7.2 μ_B whereas in Ho(FeMn), μ_{Ho} was 10.3 μ_B. These results are explained in terms of a covalent effect where the magnetic moment density is transferred from the Mn to the Ho atoms. In the case of $HoMn_2$ the transferred density is coupled antiparallel to the Ho moment which reduces the net Ho moment, whereas in Ho(FeMn) the transferred moment is polarized by the Fe moment such that is is coupled parallel to the Ho moment, making the Ho moment larger than the free ion moment and that of $HoFe_2$. Later studies performed on $HoMn_2$ by Hardman et al [12] yielded a value of 8.1 μ_B for the moment of Ho in the cubic phase and 9.4 μ_B for that of the $HoMn_2$ hexagonal phase.

Neutron scattering results for $HoFe_2$ and $HoFe_2D_{3.5}$ [14] show that the introduction of hydrogen significantly lowers the overall Curie temperature and produces a reduced moment on the rare earth site. The Ho moment drops from 10 μ_B in $HoFe_2$ to 7 μ_B in its deuteride. The weakened R-Fe and R-R exchange interactions are thought to be due to a the energy levels not being pure J_z

states due to a crystal field interaction, which reduces the sublattice moments. It has also been suggested that the observed moment may be a spatially averaged moment. The random occupation of the hydrogen sites can distort the local anisotropy field, resulting in a fanning of the rare earth moments. In contrast, the Ho moments in $Ho_6Fe_{23}D_x$ (x = 1.5, 8.2 and 15.7) remain close to 10.0 μ_B [17]. In $DyFe_4Al_8$ and $HoFe_4Al_8$ no magnetic ordering is observed in the rare earth sublattice even at 4.2K [10].

Neutron diffraction studies performed on Ho_6Mn_{23} at 77K show that at this temperature the Ho moment has a very low value of 3.8 μ_B. It is estimated that at 4K its value is around 7 μ_B or less. Thus it appears that the low moments observed for the deuteride are partly a consequence of deuteration, and partly due to disorder in the parent compound. Deuteration could lower the moment in one of two ways, either by electron transfer from the deuterium atoms which act as electron donors to the Ho^{3+} atoms, or by decreasing the average moment by creating more disorder. Since the 4f shell of the Ho^{3+} atom is more than half filled, transfer of electrons from the deuterium atoms would pair up more electrons and cause the net moment to decrease. Malik et.al. [31] have suggested that deuteration causes changes in the electronic band structure, which result in large changes in magnetic ordering in the intermetallic compound. The non-deuterated Ho_6Mn_{23} compound has a relatively high Curie temperature, T_c= 434K, which upon deuteration yields an antiferromagnetic compound $Ho_6Mn_{23}D_{22}$ with a relatively low ordering temperature, T_N, of approximately 100K. Since transition metal- transition metal interactions are predominant, T_c and T_N would correspond to ordering of the transition metal sublattice. The rare earth sublattice would order at a lower temperature. It is possible that, since the Neel temperature for $Ho_6Mn_{23}D_{22}$ is relatively low, the Ho moments are not completely ordered at 9K.

The neutron diffraction results indicate that the onset of magnetic order causes a structural distortion. The distortion does not seem to depend on the nature of the rare earth atom. Since such a structural distortion does not occur with the ordering of the non-deuterated compound, the deuterium atoms must be playing a role in the structural transformation.

III. MAGNETIC STRUCTURES OF $Y_6(Fe_xAl_{1-x})_{23}$ COMPOUNDS

A. INTRODUCTION

Y_6Fe_{23} is known to be a ferromagnet [32], which crystallizes in the Th_6Mn_{23}-type structure, space group Fm3m. It has a Curie temperature of 478K, a mean magnetic moment per iron atom of 1.88 μ_B and a bulk magnetization of 43.1 μ_B mol^{-1}. When small amounts of Mn are substituted for Fe in Y_6Fe_{23}, the bulk magnetization and the Curie temperature are observed to decrease dramatically.

Neutron diffraction studies of $Y_6(Fe_{1-x}Mn_x)_{23}$ compounds above the ordering temperatures show a marked preference of Mn atoms for the f_2 sites and Fe atoms for the f sites throughout the ternary system [33-35]. The site preference has been attributed to a volume effect; the f_1 site, having a smaller atomic volume than the f_2 site, can accommodate the smaller Fe atom more easily. On the basis of the observed preferential ordering, the striking decrease in magnetization is explained as due to the disruption of the exchange forces of the iron sublattice by Mn atoms.

The crystal structure and bulk magnetic properties of $Y_6(Fe_{1-x}Al_x)_{23}$ compounds have been studied by Besnus et al [36]. Up to about x = 0.2, the resulting ternaries are single phased. When Al is substituted for Fe, the Curie temperatures and moments decrease, not as markedly as for the $Y(Fe,Al)_2$ series nor as previously stated for Mn substitution for Fe in Y_6Fe_{23}. For an Al content of about 20%, M is decreased about 25%. The authors propose a localized model wherein the iron atoms are equivalent and possess the same mean moment as in Y_6Fe_{23}, 1.88 μ_B when they have at least seven nearest iron neighbors out of nine. The Al atoms are assumed to be stoichiometrically distributed among the four non-equivalent crystallographic sites. On these

40

bases, the spontaneous magnetization is related to those magnetic Fe atoms which have seven or more nearest Fe neighbors and no moment is assumed for those Fe atoms which have less than seven. In essence the decrease of the mean iron moment is attributed to a loss of moment as a result of the insertion of the nonmagnetic Al atoms and the non-contribution to ferromagnetism by iron atoms having less than a critical number of nearest neighbors.

Accordingly, we have carried out powder neutron diffraction studies of three $Y_6(Fe_{1-x}Al_x)_{23}$ compounds, $x = 0.05$, 0.10, and 0.15, to determine if the decrease in the magnetization resulted in part from an ordered distribution of the Al atoms, and if so, whether the smaller Al atoms would prefer the f_1 site of smaller atomic volume relative to the f_2 site.

B. EXPERIMENTAL

The samples of $Y_6(Fe_{1-x}Al_x)_{23}$ were prepared by induction melting of the elements in the appropriate stoichiometric amounts in a water cooled, copper cold boat under an argon atmosphere. These were annealed in vacuo at 900°C for one week. X-ray diffraction patterns exhibited only lines belonging to the face-centered cubic (Fm3m) single phase. Neutron diffraction data above T_c and at 77K were collected at the University of Missouri Research Reactor at Columbia ($\lambda = 1.293$). The data were analyzed using a modified Rietveld profile technique [27]. In the refinement of the data, no constraints were used for the total Fe and Al content, but a constraint was imposed such that the sum of the Fe and Al atoms would produce full occupancy at each transition metal site.

C. RESULTS AND DISCUSSION

Preferred Site Occupancy of Fe and Al Atoms

At 523K, the $Y_6(Fe_{1-x}Al_x)_{23}$ intermetallic compounds exhibit no long-range magnetic ordering. The structural parameters derived from the modified Rietveld refinement program, assuming space group Fm3m (Oh^5) are given in Table XIII. The e site is occupied by Y (6 atoms), while Fe and Al occupy the sites b (1 atom), d (6 atoms), f_1 with x = 0.176 (8 atoms), and f_2 with x = 0.378 (8 atoms). The results show the presence of preferential site ordering in all three systems. In all cases, the R factors and values for those refinements which show preferential site ordering are considerably less than those in which Al and Fe are assumed to be stoichiometrically distributed at each site.

As shown in Fig. 6, the Fe atoms prefer the f_1, d, and b sites, whereas Al prefers the f site. Within the limits of experimental error, only Fe atoms occupy the f_1 site. A comparison of the atomic volumes and nearest neighbor distances of these sites provides an insight for this site preference. The nearest neighbor distances for each of the four transition metal sites are given in Table XIV. The f_1 site has nine nearest neighbor transition metal sites of which three f_1 sites and three d sites lie at a distance of 2.47A and 2.48A respectively. The d site has three f_1 neighbors at a distance of 2.48A whereas the closest neighbors of the f site lie at a distance of 2.55A. The preference of Al for the f_2 site cannot be only a consequence of the atomic volume of the f2 site inasmuch as its atomic volume is larger than that of the f_1 site which is occupied almost exclusively by the larger Fe atoms. The site preference may arise more as a consequence of bonding considerations.

TABLE XIII

OCCUPATION OF ATOMS IN CRYSTALLOGRAPHIC SITES OF
$Y_6(Fe_{1-x}Al_x)_{23}$ COMPOUNDS

	x=0.05 No. (%)	x=0.10 No. (%)	x=0.15 No. (%)
Al_b	0.049(4.90)	0.055(5.50)	0.059(5.90)
Fe_b	0.951(95.10)	0.945(94.50)	0.940(94.10)
Al_d	0.228(3.80)	0.232(3.86)	0.237(3.95)
Fe_d	5.772(96.20)	5.768(96.14)	5.763(96.05)
Al_f	0.011(0.13)	0.027(0.34)	0.029(0.37)
Fe_f	7.989(99.87)	7.973(99.66)	7.969(99.63)
Al_f	0.989(11.36)	2.178(27.22)	3.168(39.60)
Fe_f	7.091(88.64)	5.822(72.78)	4.831(60.40)
Al_{Total}	1.197(5.21)	2.492(10.83)	3.493(15.18)
Fe_{Total}	21.802(94.79)	20.508(89.17)	19.503(84.82)
$R_{nuclear}$	1.10	1.94	1.23
$R_{overall}$	2.49	3.18	2.67
R_{random}	4.19	8.94	13.34
$R_{expected}$	1.21	1.25	1.44
X	2.05	2.54	1.88
X_{random}	3.46	7.15	9.26
x	0.0521	0.108	0.152
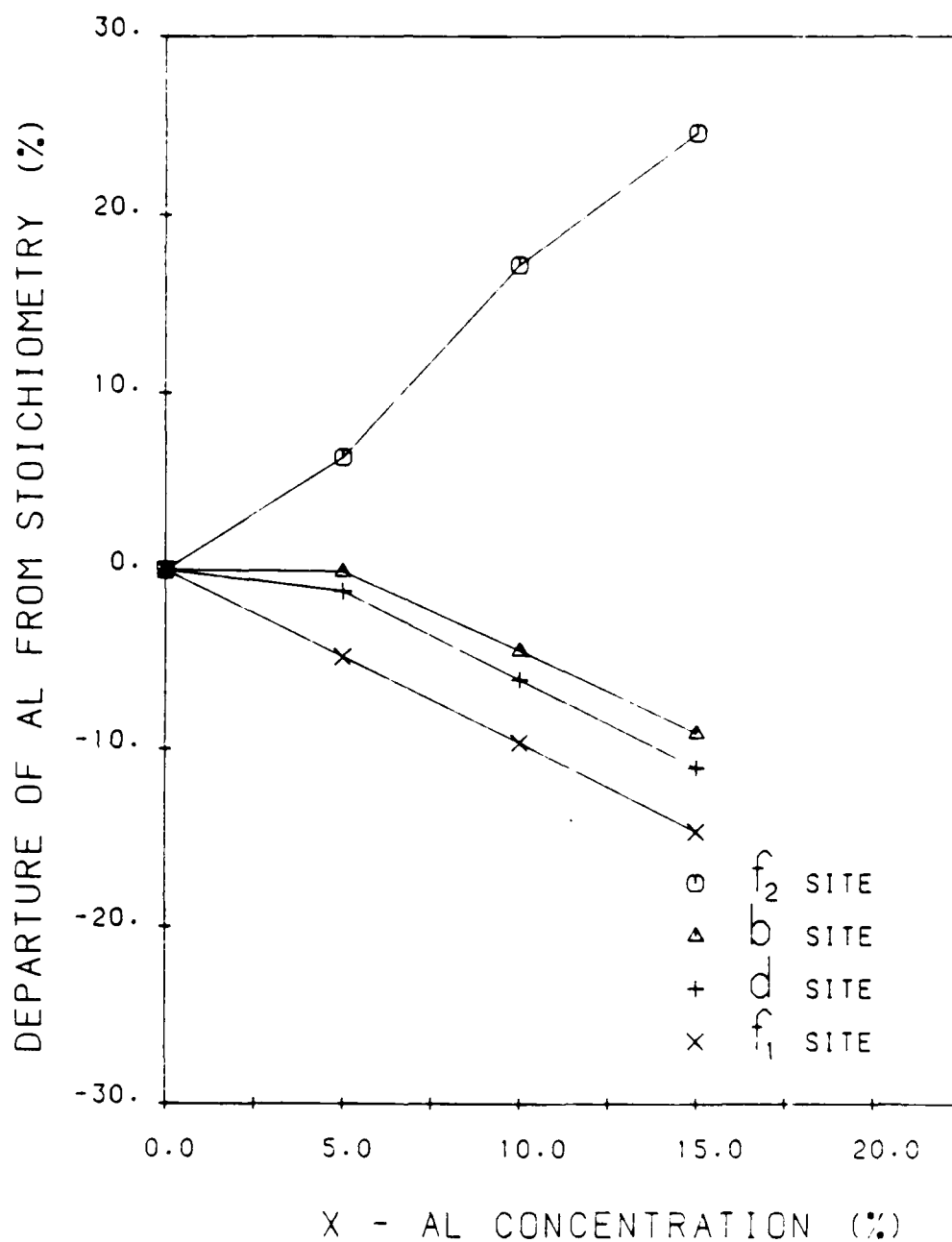
Figure 6. Prefential site ordering in $Y_6(Fe_{1-x}Al_x)_{23}$ compounds, expressed as a percentage departure from a stoichiometric distribution.

TABLE XIV. Nearest Neighbor Distances of
$Y_6(Fe_{0.95}Al_{0.05})_{23}$ at 77K

Site	Distance A (^{1} .001)	No. of Atoms
f_1-f_1	2.474	3
f_1-d	2.478	3
f_2-b	2.546	1
f_1-f_2	2.631	3
f_2-d	2.656	3
d-d	3.032	1
b-d	4.293	3
f_2-f_2	4.427	3
f_1-b	4.96	3
b-b	8.574	3

Specifically, the f_1 site nearest neighbors constitute a total of nine, wherein the nearest neighbor distances are 2.47, 2.48, and 2.63Å for the f_1-f_1, f_1-d, and f_1-f_2 bonds, respectively. If one takes into account the percentage of iron atoms at each site for the alloy containing 10% Al, the effective number of Fe atom nearest neighbors is relatively high, approximately eight. For the f_2 site, there are nearly seven nearest neighbors with bond distances of 2.55, 2.63, and 2.66Å corresponding to f_2-b, f-f, and f-d, respectively. Accordingly, if a localized model is assumed, the higher occupancy of the f_1 site by Fe atoms, permits a greater overlap of their bonding orbitals with a greater number of nearest neighbors resulting in a more stable structure.

This may also explain the site preference observed for the $Y_6(Fe_xMn_{1-x})_{23}$ compounds. If the larger atomic volume of the f_2 site were the governing factor for the site preference of Mn, then in the $Y_6(Fe_{1-x}Al_x)_{23}$ compounds, one might expect to find the smaller Al atoms favoring the f site. Models which assigned a majority of Al atoms in the f site yielded poor profile fits to the neutron diffraction data.

Magnetic Structures of $Y_6(Fe_{1-x}Al_x)_{23}$ Compounds at 77K

As shown in Table XV, the magnetic moments of the Fe atoms, which lie along the <111> direction, are coupled ferromagnetically with different magnetic moments at each of the four transition metal sites. The magnetic moment of Fe at the f_1 site decreases markedly with increasing percentage of Al in the compound, while little change is observed at the other three sites, Fig. 7.

In many compounds, the long range magnetic ordering of the Fe moments is dependent on the local chemical environment of these atoms [35,36]. When Al is added to Y_6Fe_{23}, the change in atomic ordering in the $Y_6(Fe_{1-x}Al_x)_{23}$ system

46

TABLE XV

ATOMIC ORDERING AND SITE MAGNETIZATION OF SOME $Y_6(Fe_{1-x}Al_x)_{23}$ COMPOUNDS

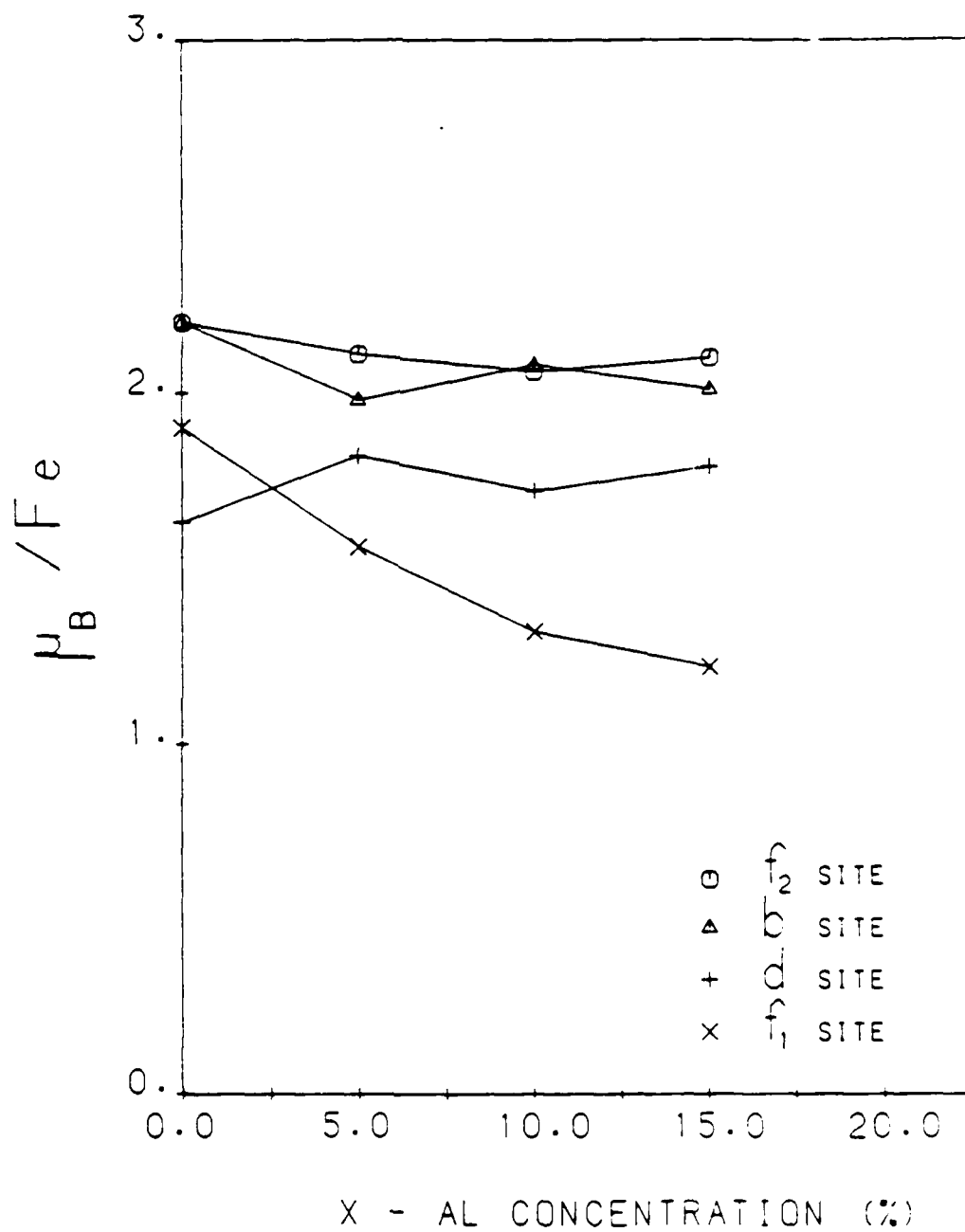| Site	x=0	x=0.10	x=0.20	x=0.27
b %Mn		9.5	20.9	31.9
d %Mn		5.7	11.7	17.8
f_1 %Mn		2.6	6.8	11.1
f_2 %Mn		20.3	37.4	47.6
b μ_b/Fe moment	2.2	2.2	1.80	0.75
d μ_b/Fe moment	1.63	1.78	1.05	0.53
f_1 μ_b/Fe moment	1.90	1.43	0.54	0.00
f_2 μ_b/Fe moment	2.2	2.20	1.80	0.99
$T(K)$[*]	78	4	12	4
a_o(A)	12.055	12.058	12.067	12.083

[*] Temperatures at which the data were taken.

Figure 7. Fe magnetic moments in $Y_6(Fe_{1-x}Al_x)_{23}$ compounds.

can affect the local environment of the Fe atoms and lead to changes in magnetic order. The magnetic moment of Fe at the f_2 site hardly changes as x is varied. This is to be expected as the atomic volume of this site is large, and there is a smaller overlap of Fe orbitals with those of the neighboring sites. This also explains the large magnetic moment of Fe at this site. Since the f_1 site has six nearest neighbors ($3f_1$ and 3d) which lie at a distance of 2.47A, the effects of the Al diluent on the magnetic moment of Fe should be felt most at this site. The refinement results do show a drop in the magnetic moment of Fe at the f_1 site with increasing Al concentration. The d site too has three of its nearest neighbors (f_1) at a distance of 2.5A. Therefore, the magnetic moment of Fe at this site is expected to decrease with increasing Al concentration, although not to the extent as that at the f_1 site. Within experimental error, our results show no change. The relatively large error limits of the magnetic moments might well hide a small change in moment. It is noted that the Fe moment at the b site remains essentially constant due to the presence of nearest neighbor Fe atoms on the f_2 site. Since the b site contributes only 1 atom/f.u., the refined magnetic moments at this site carry larger errors than those at the other sites, see Table XVI.

On the basis of the neutron diffraction results, the decrease in the Curie temperatures and bulk magnetizations of the $Y_6(Fe_{1-x}Al_x)_{23}$ series arises as a result of two effects, dilution of the total magnetization resulting from the insertion of nonmagnetic atoms and the changes in atomic ordering which affect the local environments of the Fe atoms and lead to a decrease in overall Fe moment. The major decrease in the average Fe moment occurs at the f_1 site.

TABLE XVI

MAGNETIC MOMENTS AT CRYSTALLOGRAPHIC SITES OF $Y_6(Fe_{1-x}Al_x)_{23}$ COMPOUNDS
AT 77K

Site	x=0	x=0.05	x=0.10	x=0.15
b	2.20	1.98±0.6	2.08±0.6	2.01±0.6
d	1.63	1.82±0.1	1.72±0.1	1.79±0.1
f_1	1.90	1.56±0.1	1.34±0.1	1.22±0.1
f_2	2.20	2.11±0.1	2.06±0.1	2.10±0.1
Calculated bulk moment (μ/f.u.)	44.78	39.81	35.55	32.08
Experimental bulk moment (μ/f.u.)*	43.32	40.39	34.7	31.16
R_{mag}	2.67	1.65	1.65	1.84

* Measured at 4.2K [44].

The neutron diffraction results indicate that the onset of magnetic order causes a structural distortion. The distortion does not seem to depend on the nature of the rare earth atom. Since such a structural distortion does not occur with the ordering of the non-deuterated compound, the deuterium atoms must be playing a role in the structural transformation.

IV. A MOSSBAUER EFFECT STUDY OF THE MAGNETIC ORDERING IN
$Y_6(Fe_xMn_{1-x})_{23}$ ALLOYS

A. INTRODUCTION

Because certain rare earth-transition metal intermetallic alloys combine a high magnetocrystalline anisotropy with high magnetization, they exhibit the properties of good permanent magnets [37]. Materials of this type have been studied not only for their unusual magnetic behavior, but more recently, because of their ability to absorb, store, and desorb large quantities of hydrogen [38]. This paper directs its attention to the $Y_6(Fe_xMn_{1-x})_{23}$ ternary system and the magnetic properties it demonstrates.

These ternary alloys exhibit anomolous magnetic behavior relative to their end members, Y_6Fe_{23} and Y_6Mn_{23} [39]. Although Y_6Fe_{23} and Y_6Mn_{23} are respectively, ferromagnetically and antiferromagnetically ordered at room temperature, their ordering temperature and magnetization decrease markedly with increasing manganese content in Y_6Fe_{23} and with increasing iron content in Y_6Mn_{23} [39]. For values of x between 0.5 to 0.75 the magnetic ordering temperature is reported by Kirchmayr and Steiner [39] to have virtually vanished. Further, Long et al. [40] have reported the absence of any ordering in $Y_6(Fe_{0.2}Mn_{0.8})_{23}$ and $Y_6(Fe_{0.1}Mn_{0.9})_{23}$ down to ca. 1.4K.

The crystal structure of $Y_6(Fe_xMn_{1-x})_{23}$ is face centered cubic (Fm3m), is isostructural with Th_6Mn_{23}, and has 116 atoms per unit cell. It contains an octahedral cluster of six yttrium atoms on each cubic face. This cluster is surrounded by fifty transition metal atoms which occupy four nonequivalent

lattice sites containing iron or manganese and designated as b, d, f_1, and f_2 with degeneracies of 1, 6, 8, and 8, respectively [41]. X-ray diffraction studies of lattice parameters have indicated a negative deviation from Vegard's law [1], suggesting that the electronic environment of each transition metal site is different. Iron-iron interactions are ferromagnetic and compete with iron-manganese interactions which are antiferromagnetic [34].

Hardman, et al. [34] report that there is a degree of preferential ordering on the f_1 and f_2 sites in these ternary alloys. Neutron diffraction results [34] show that the addition of manganese to Y_6Fe_{23} produces a higher concentration of manganese than expected on the f_2 site. Concurrently, the f_1 site shows preferential occupation by iron atoms.

B. EXPERIMENTAL

All compounds were prepared by induction melting of stoichiometric amounts of 99.9 percent pure elements in a cold copper boat under an argon atmosphere. The samples were annealed in a resistance furnace for four days at 1173K under a 10^{-5} torr vacuum. X-ray diffraction results showed the samples were single phase alloys.

Mossbauer spectra were obtained at ambient temperature, 78, 4.2, and 1.3K on a Harwell or a Ranger constant acceleration spectrometer which utilized a room-temperature rhodium-matrix source and was calibrated at room temperature with natural abundance α-iron foil. Spectra obtained at 4.2K and below were measured in a cryostat in which the sample was placed directly in the liquid helium and the sample temperature was obtained from the helium vapor pressure.

The Mossbauer spectra were fit to Lorentzian lines by using least-squares minimization techniques. Magnetic spectra were fit to four hyperfine sextets each with an adjustable isomer shift, δ, internal hyperfine field, H_{int}, and

line width, Γ, which was the width of the innermost lines. The line widths of lines 2 and 5 were $\Gamma+0.5\Delta\Gamma$ and the line widths of lines 1 and 6 were $\Gamma+\Delta\Gamma$, where $\Delta\Gamma$ was determined from preliminary fits. Relative areas of the lines in each component were constrained in the ratio of 3:2:1:1:2:3 as is required for a randomly oriented powder sample. The relative areas for each spectral component were constrained to the relative occupation values determined from neutron diffraction refinements on these ternary alloys [34]. Paramagnetic spectra were fit to symmetric quadrupole doublets whose areas were constrained to the same occupation values. The b site was constrained to be a singlet with a constant isomer shift equal to 0.03mm/s.

C. RESULTS AND DISCUSSION

Many rare earth-transition metal alloys show some degree of long range magnetic order. The nature of this ordering is usually dependent upon the local chemical environment of the magnetic atoms and the various competing exchange interactions. The magnetic ordering in $Y_6(Fe_xMn_{1-x})_{23}$ has been shown to have local coordination effects.

In our work, the amount of iron versus manganese on each site is constrained to values determined from neutron diffraction refinements [34]. Mossbauer spectra were obtained for the $Y_6(Fe_xMn_{1-x})_{23}$ alloys where x is 1.00, 0.90, 0.81, 0.74, 0.59, and 0.52, and the results obtained at 1.3K are illustrated, in part, in Figure 8. The results obtained for $Y_6(Fe_{0.81}Mn_{0.19})_{23}$ as a function of temperature are shown in Figure 9. Long range magnetic ordering occurs for all the alloys at 4.2 and 1.3K. As the temperature is increased to 78K, only the alloys with x greater than 0.81 show long range magnetic order on the iron sites. At room temperature only Y_6Fe_{23} and $Y_6(Fe_{0.90}Mn_{0.10})_{23}$ exhibit such long range magnetic order.
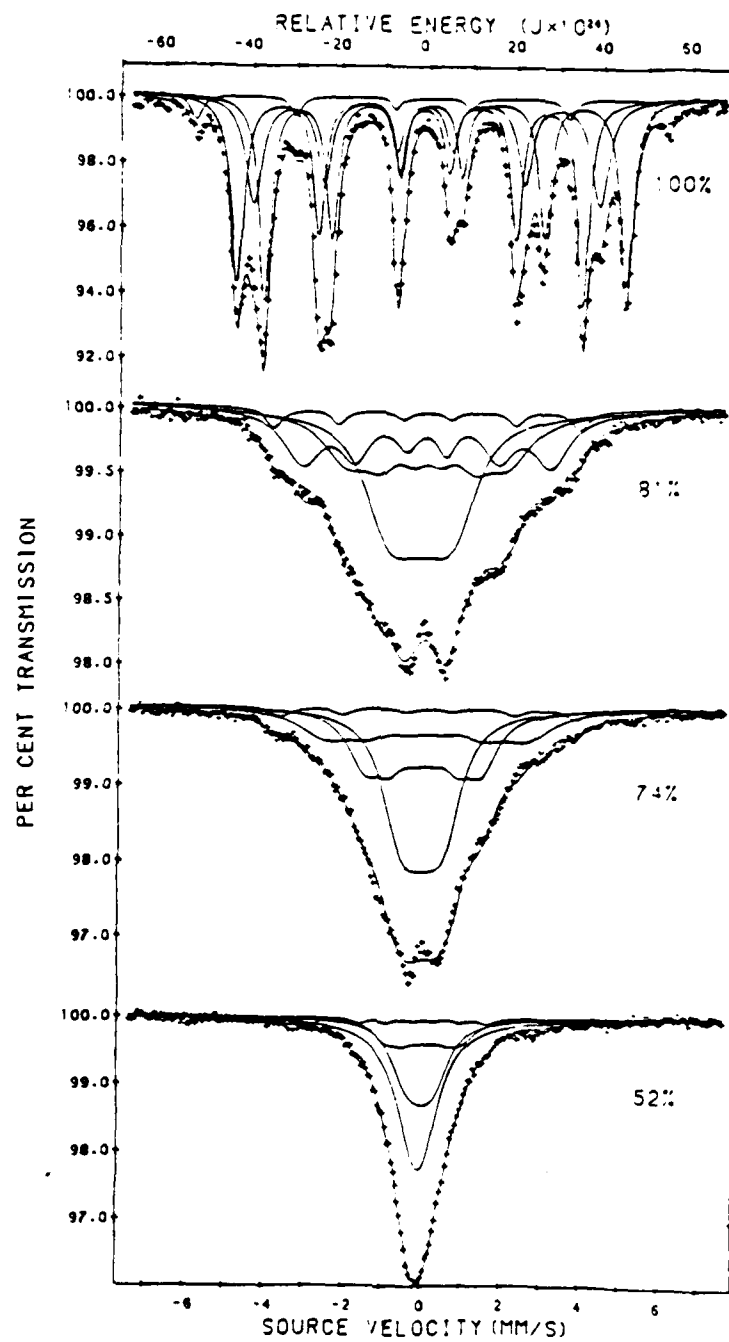
Figure 8. The Mossbauer effect spectra of several
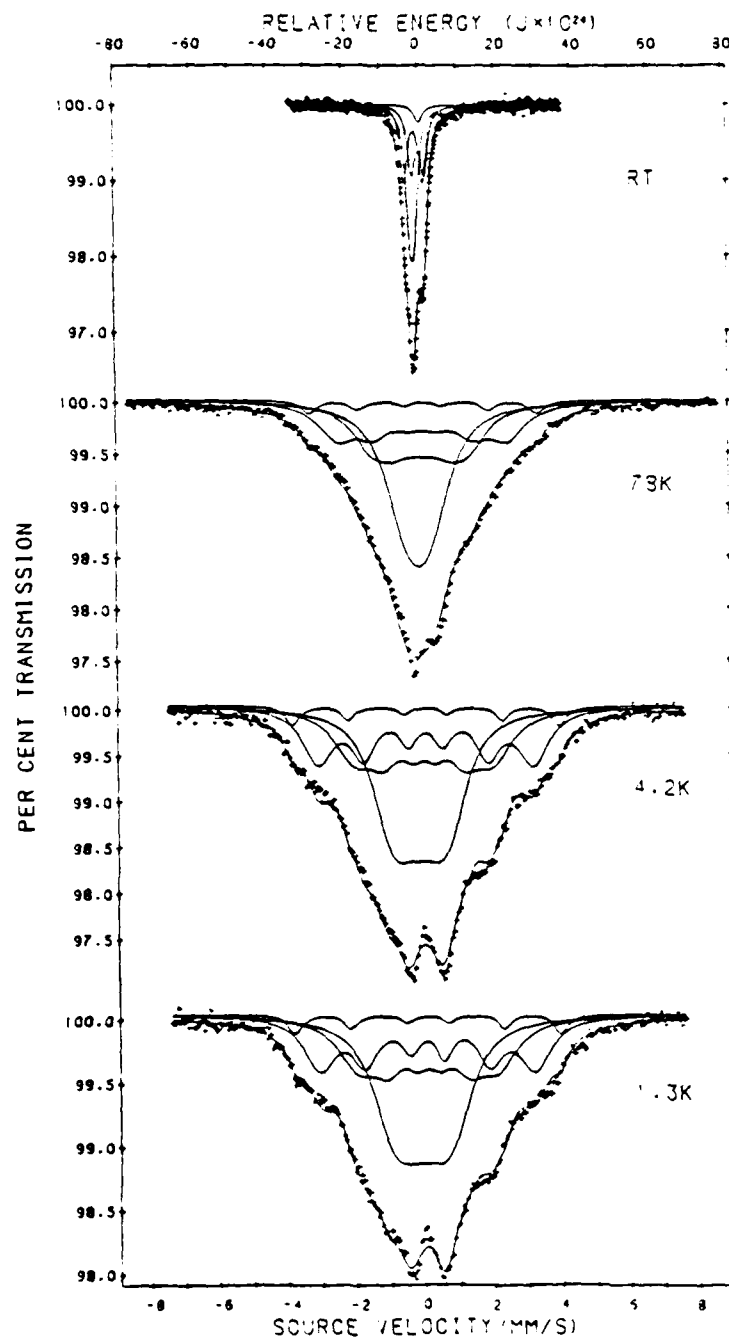Y_6 $(Fe_xMn_{1-x})_{23}$ alloys obtained at 1.3K.

Figure 9. The Mossbauer effect spectra of $Y_6(Fe_{0.81}Mn_{0.19})_{23}$ obtained at several temperatures.
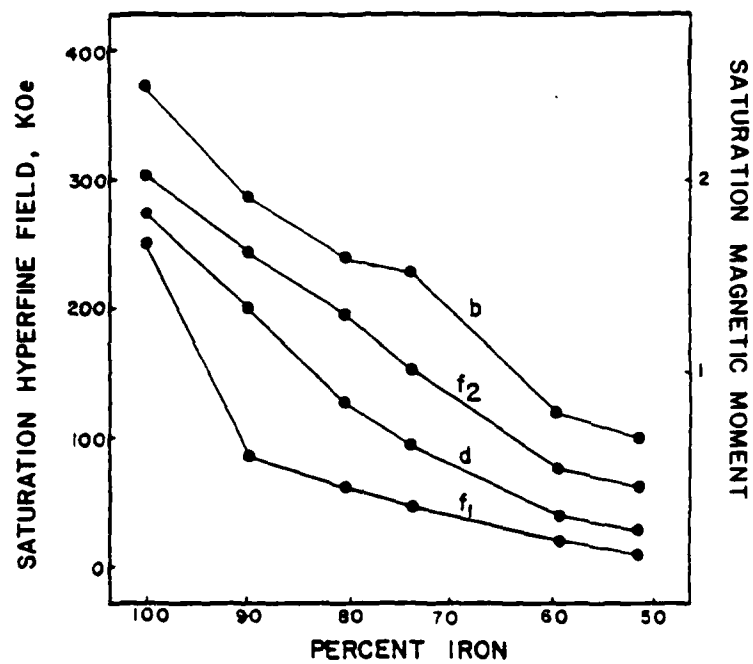
Figure 10. The saturation hyperfine field and moment of $Y_6(Fe_xMn_{1-x})_{23}$ as a function of composition.

Y_6Fe_{23} was initially used to determine the heirarchy of magnetic moments and hence the heirarchy of hyperfine field values for each spectrum. Best fits were obtained when the order of the fields was taken as $b > f_2 > d > f_1$. Isomer shift values followed the same trend, whereas the quadrupole shift values were constrained to zero, because each site is close to cubic symmetry.

The Mossbauer spectra show that each crystallographic site exhibits a unique hyperfine field. In Y_6Fe_{23} the iron moments couple ferromagnetically [34], and this coupling is weakened upon addition of manganese. As a result, the Curie temperature and magnetization decrease due to the antiferromagnetic coupling of the b and d sites with the f_1 and f_2 sites. A plot of internal hyperfine fields, and the corresponding moments, at 1.3K versus composition is shown in Figure 10. The decrease in the hyperfine fields agrees well with the decreasing magnetic moments observed by neutron diffraction [34]. This decrease apparently results from the increasing frustration of the ferromagnetic iron-iron coupling as additional manganese, which would prefer antiferromagnetic coupling, both with itself [7] and with iron [34], is introduced into the alloys.

V. MAGNETIC PROPERTIES OF SUBSTITUTED $R_2(Fe,Al,Co)_{14}B$
COMPOUNDS

A. INTRODUCTION

The permanent magnets based on $Nd_2Fe_{14}B$ compounds exhibit the highest energy product. The Curie temperatures are, however, low. Earlier work [42,43] has shown that substitution of Fe with Co results in an increasing Curie temperature, but a decreasing coercivity. The heavy rare earths, e.g., Dy or Tb, enhance the coercivity, but decrease the magnetization because of ferrimagnetic coupling between the heavy rare earth and iron. To improve the temperature stability of, and to reduce reversible and irreversible losses in, the Nd-Fe-B magnets, we need to increase both Curie temperature and coercivity, while retaining the high energy product. It is with this objective that we have undertaken a study of the effects of substitution of Fe by other elements on the intrinsic and permanent magnetic properties of $R_2Fe_{14}B$ systems.

$R_2Fe_{14}B$ crystallizes in a tetragonal structure in which Fe atoms are distributed over six non-equivalent sites. It is expected that substitution of Fe by other atoms will occur with preferred atomic ordering such that the changes in nearest neighbor interactions may give rise to important changes in both the nuclear and magnetic structures and in the metallurgical micro-structure.

B. EXPERIMENTAL

The samples were prepared by arc-melting of 99.9% pure primary materials followed by vacuum annealing at a temperature of 700°C for 6 hours. The single phase was identified from X-ray diffraction patterns and thermomagnetic

59

analyses. To study the permanent magnet performance, the magnets were prepared with a composition of $Nd_{16.5}Fe_{76.5}B_7$, sintered at 1090°C, and followed by a post-annealing at 700°C. The samples were cylindrical with a ratio of length to diameter = 1.

The Curie temperatures were measured from room temperature to 700°C using a magnetic balance. The extraction method was used to measure the saturation magnetization and magnetocrystalline anisotropy in a superconducting field up to 70 kOe, and in a temperature range 1.5K to 300K. In order to measure the magnetocrystalline anisotropy, the ingots were ground to provide an average grain diameter of less than 30 μm and the grains were then oriented at room temperature in a magnetic field of 10 kOe. Magnetization curves were measured on aligned samples in, and normal to, the alignment direction.

C. RESULTS AND DISCUSSION

X-ray diffraction studies indicate that $R_2(Fe_{1-x}Al_x)_{14}B$ crystallizes in the tetragonal structure, space group $P4_2/mnm$ when $x < 0.1$. When $x > 0.1$, a second phase of a significant amount is observed both metallographically and in the X-ray patterns. Lattice measurements demonstrate the cell volume decreases with increasing Al content, x. That suggests that Al is replacing Fe rather than B.

1. Intrinsic Magnetic Properties of $Y_2(Fe_{1-x}Al_x)_{14}B$

Curie Temperature, T_c. The compositional dependence of the Curie temperature, T_c, is shown in Figure 11. T_c decreases monotonically with increasing x, indicating a weakening of the magnetic interaction, resulting from the dilution with non-magnetic Al atoms. In $Y_2(Fe_{1-x}Al_x)_{14}B$ compounds, Y, Al, and B are non- magnetic. The T_c is, therefore, completely controlled by Fe-Fe exchange interactions. Therefore, if Al is substituted for Y or B, the Curie temperature should be insensitive to Al insertion. The fact that T_c
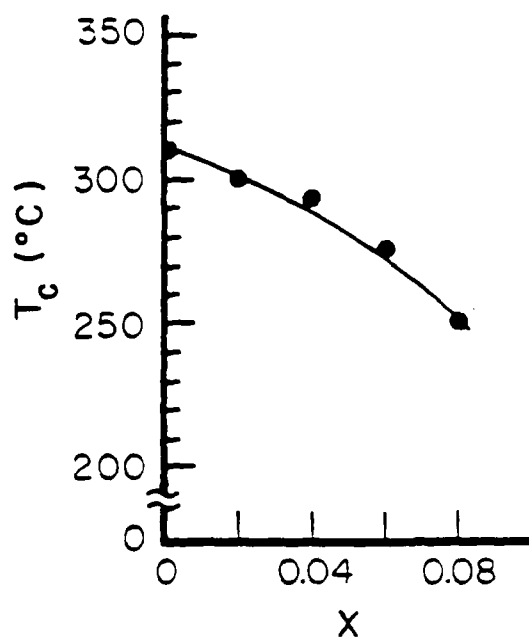
Figure 11.   Composition dependence of Curie temperature
T_c of $Y_2(Fe_{1-x}Al_x)_{14}B$.

Table XVII.   Saturation magnetization, σ, and average
atomic moment, μ, of Fe in $Y_2(Fe_{1-x}Al_x)_{14}B$
at 1.5K.

x	σ (emu/g)	μ (μB/atom)
0.00	156.0	1.94
0.02	148.6	1.39
0.04	144.2	1.79
0.06	134.8	1.71
0.08	129.2	1.65

decreases with increasing Al content provides further evidence for the concept that Al enters the Fe sublattice.

Saturation Magnetization at 1.5K. Table XVII shows the variation of saturation magnetization as a function of Al content, x. The rate of the decrease is much larger than that expected from simple dilution. The average Fe atom moment decreases with increasing Al content.

Magnetocrystalline Anisotropy. The magnetization curves along the easy and hard directions were measured at 1.5K. The anisotropy constant, K_1 and K_2, were estimated from the magnetization curves using the Sucksmith-Thompson method [44]. Figures 12 and 13 show the variation of the anisotropy constants, K_1 and K_2, and the anisotropy field, H_A, with Al content, x.

The increase of K_1 and H_A as Fe is substituted by Al in these compounds is of particular interest. In the $R_2Fe_{14}B$ structure, Fe atoms are distributed on six crystallographically non-equivalent sites which are designated as Fe(c), Fe(e), Fe(j), Fe(K_1), and Fe(K_2). According to Herbst et al., [45] the Fe(j_2) atoms in $R_2Fe_{14}B$ and the Fe(c) atoms in R_2Fe_{17} are cognate both crystallographically and magnetically. Each Fe(j_2) atom has twelve Fe neighbors in a highly symmetric geometry which should promote a planar tendency in terms of the magnetization direction. Accordingly, the increase of uniaxial anisotropy with the addition of Al suggests that Al substitutes preferentially on the j_2 sites. This suggestion is consistent with the saturation magnetization data inasmuch as the Fe(j_2) moment is the largest [45]. Neutron diffraction and Mossbauer spectrum studies are now in progress to determine the location of the Al atoms.

2. Coercivity of $Nd_{16.5}(Fe_{1-x}Al_x)_{73.5}B_7$

The addition of Al significantly enhances the coercivity. Figure 14 shows the compositional dependence of the intrinsic coercivity of Nd_{16}
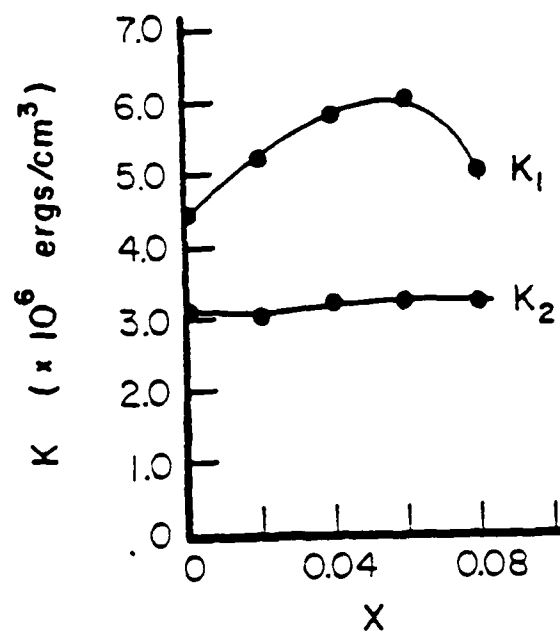
Figure 12.   Variation of anisotropy constants, K_1 and K_2, with x of $Y_2(Fe_{1-x}Al_x)_{14}B$.
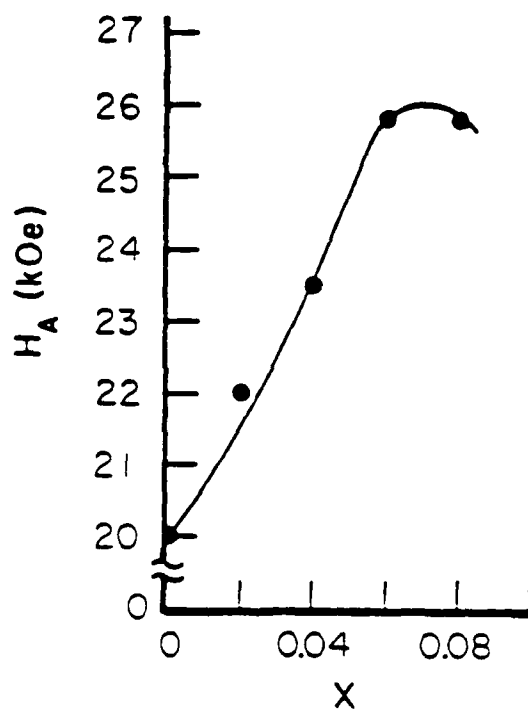

Figure 13.   Variation of anisotropy field, H_A, with x of $Y_2(Fe_{1-x}Al_x)_{14}B$.
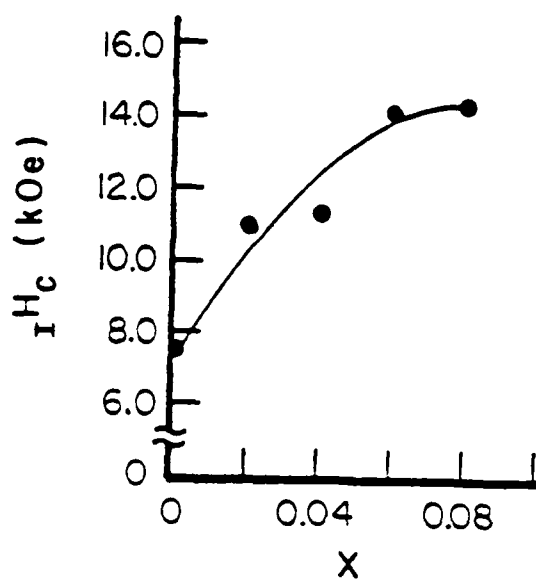
63

Figure 14. Composition dependence of intrinsic coer-
civity, H_c, of $Nd_{16.5}(Fe_{1-x}Al_x)_{76.5}B_7$.

Table XVIII. Permanent magnetic properties of
$Nd_{16.5}(Fe_{1-x}Al_x)_{76.5}B_7$

x	B_r(G)	$_iH_c$(Oe)	$(BH)_m$(MGOe)	T_c °C
0.0	13000	7500	37.8	330
0.02	12100	10900	34.5	320
0.04	11200	11300	30.0	307
0.06	10900	14100	27.8	298
0.08	9300	14300	19.3	289

$_s(Fe_{1-x}Al_x)_{7s}$ $_sB_7$, at room temperature. Table XVIII summarizes the permanent magnetic properties of Nd_{16} $_s(Fe_{1-x}Al_x)_{7s}$ $_sB_7$.

The increase of coercivity may result from a change in the crystalline or metallurgical microstructure due to the Al insertion. As Livingston [46] has pointed out, the coercivity in sintered Nd-Fe-B magnets is "nucleation-controlled" (as in the $SmCo_s$ magnets) [46]. Even in nucleation-controlled magnets, the pinning of domain walls by grain boundaries is necessary to provide a barrier to the propagation of magnetization reversal from grain to grain. The addition of Al to Nd-Fe-B magnets may create or influence another phase along the boundaries. However, the effect of replacing Fe by Al atoms on the intrinsic magnetic properties of the principal phase may be related also to the coercivity, in that Al insertion enhances the anisotropy and weakens the exchange interaction. That should result in thinner domain walls, thus favoring the pinning of domain walls at the grain boundaries.

3. Permanent Magnetic Properties of Substituted Nd-(Fe,Al,Co)-B Magnets

Addition of Al to the Nd-Fe-B magnets increases the coercivity, but unfortunately decreases the Curie temperature and saturation magnetization. Earlier work has shown that the substitution effect of Fe by Co can make up for this loss. Table XIX summarizes the performance of the magnets based on the composition Nd_{16} $_s(Fe_{1-x-y}Al_xCo_y)_{76}$ $_sB_7$. Table ddd indicates that the thermal magnetic properties are improved and that the total loss is reduced. By manipulation of the stoichiometric ratios of Nd, Al, and Co, it may possible to produce a magnet with a T_c ≈500°C, $_iH_c$ > 10 kOe, and $(BH)_m$ > 30 MGOe.

Table XIX. Permanent magnetic properties of
$Nd_{16.5}(Fe_{1-x-y}Al_xCo_y)_{76.5}B_7$

x	y	B_r (kG)	$_iH_c$ (kOe)	BH_m (MGOe)	T_c (°C)	Irrev. Loss (%)	Rev. Loss (%)	Temp. Coeff. 20-100°C (%/°C)
0.00	0.00	13.0	7.5	37.8	310	21.62	8.55	0.113
0.00	0.26	12.9	6.0	33.3	504	19.44	5.14	0.069
0.04	0.26	11.7	9.5	31.0	492	3.12	5.79	0.078

VI. MAGNETOCRYSTALLINE ANISOTROPY OF
$(Nd_{1-x}Sm_x)_2Fe_{14}B$ AND $(Nd_{1-x}Pr_x)_2Fe_{14}B$
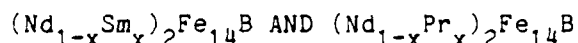
A. INTRODUCTION

A great interest has been paid to the $R_2Fe_{14}B$ compounds since the discovery of their outstanding magnetic properties [47]. Their uses are related to the properties of magnetocrystalline anisotropy. Earlier work showed a variety of magnetocrystalline anisotropy in $R_2Fe_{14}B$ compounds [48,49]. $Pr_2Fe_{14}B$ has an easy axis and $Sm_2Fe_{14}B$ has an easy plane. $Nd_2Fe_{14}B$ presents axial anisotropy at room temperature, however, a spin reorientation occurs at around 140K. A study of magnetocrystalline anisotropy and spin reorientation is, therefore, of practical as well as scientific interest. We expected to get useful information by investigating the substitution effect of Nd by Pr and Sm in this respect.

B. EXPERIMENTAL

The samples with the composition $R_{15}B_7Fe_{78}$ were prepared by arc-melting and following by vacuum annealing at 700°C. To identify the single phase, X-ray and thermomagnetic measurements were made.

Magnetization curves along easy and hard directions were measured on aligned samples with a field up to 70 KOe in a temperature range between 1.5K and 273K. In addition to the magnetic measurements, X-ray diffraction experiments performed on powdered samples aligned in a field at desirable temperature were made to determine the easy magnetization direction.

C. RESULTS AND DISCUSSIONS

A complete solid solubility exists in $Nd_2Fe_{14}B-Pr_2Fe_{14}B-Sm_2Fe_{14}B$ compounds. They crystallize in the tetragonal structure.

1. Substitution effect of Nd with Pr on magnetocrystalline anisotropy
   and spin reorientation

Magnetization curves of $(Nd_{1-x}Pr_x)_2Fe_{14}B$, x = 0.0, 0.1, 0.2, 0.3, 0.4, 0.5, 0.7, 0.8, and 1.0, were measured along easy and hard directions in a temperature range between 1.5K and 273K. As an example Fig. 15 shows the magnetization curves at 1.5K with x = 0.1 and 0.8. Anisotropy constants K_1 and K_2 are estimated by using Sucksmith-Thompson method [44]. Figure 16 shows the variation of K_1 and K_2 as a function of the Pr content x at 1.5K. These results indicate that at 1.5K the easy magnetization direction is deviated from c-axis when x < 0.6 and the cone angles θ decrease with increasing Pr content x, Fig. 17. Spin reorientation temperatures T_s decrease with substitution of Nd by Pr. When x > 0.6, c-axis is the easy axis even at 1.5K, Fig. 18.

2. Substitution effect of Nd by Sm on magnetocrystalline anisotropy and
   spin reorientation

Magnetization curves of $(Nd_{1-x}Sm_x)_2Fe_{14}B$ measured at room temperature along easy and hard directions are shown in Fig. 19. In addition to the magnetic measurements, X-ray diffraction patterns of aligned powder samples show a sharp increase of the (0,0,6) reflections and a disappearance of (3,3,0) line for the compounds with x > 0.3. When x < 0.3, the situation is reversed. Accordingly, we can conclude that at room temperature for the $(Nd_{1-x}Sm_x)_2Fe_{14}B$ compounds, the c-axis is the easy axis when x < 0.3; while the easy magnetization direction lies in the basal plane, when x > 0.3. Anisotropy field H_A, easy magnetization direction (E.M.D.) and spin reorientation temperature T_s are summarized in Table XX.

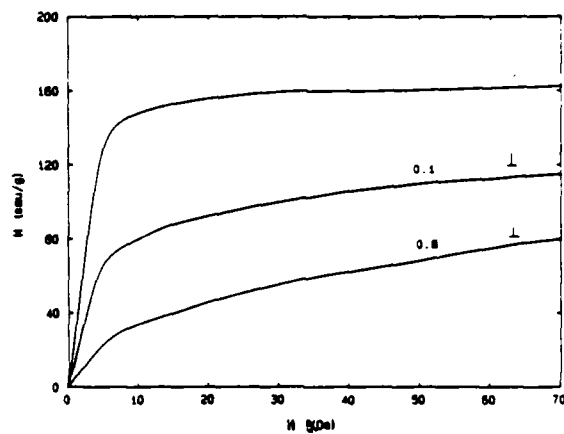Fig. 15. The magnetization curves of $(Nd_{1-x}Pr_x)_2Fe_{14}B$ at 1.5K with $x = 0.1$ and 0.8.
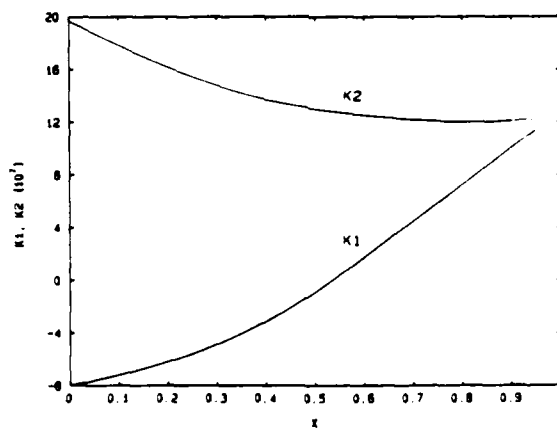
Fig. 16. The variation of K_1 and K_2 (erg/cm^3) of $(Nd_{1-x}Pr_x)_2Fe_{14}B$ as a function of the Pr content x at 1.5K.
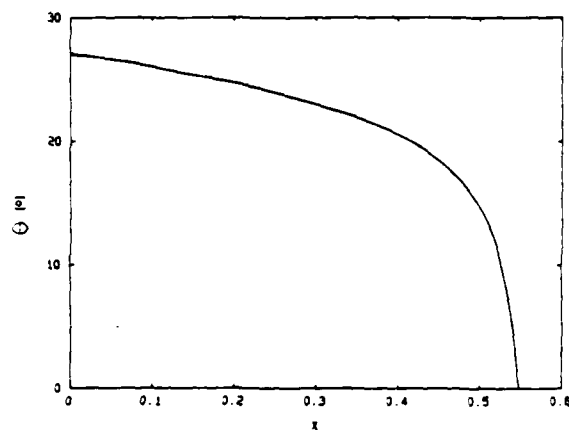
Fig. 17. The variation of the cone angles ϑ of $(Nd_{1-x}Pr_x)_2Fe_{14}B$ as a function of the Pr content x at 1.5 K.

Fig. 18. The variation of spin reorientation temperature T_s of $(Nd_{1-x}Pr_x)_2Fe_{14}B$ as a function of the Pr content x.

Fig. 19. Magnetization curves of $(Nd_{1-x}Sm_x)_2Fe_{14}B$ measured at room temperature along the easy and hard directions with x = 0.1, 0.25, 0.3 and 0.4.

TABLE XX

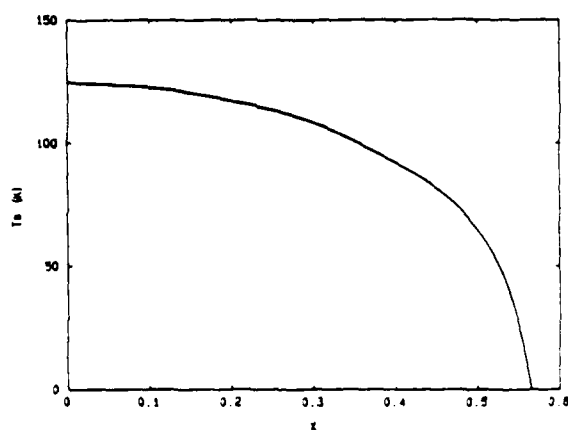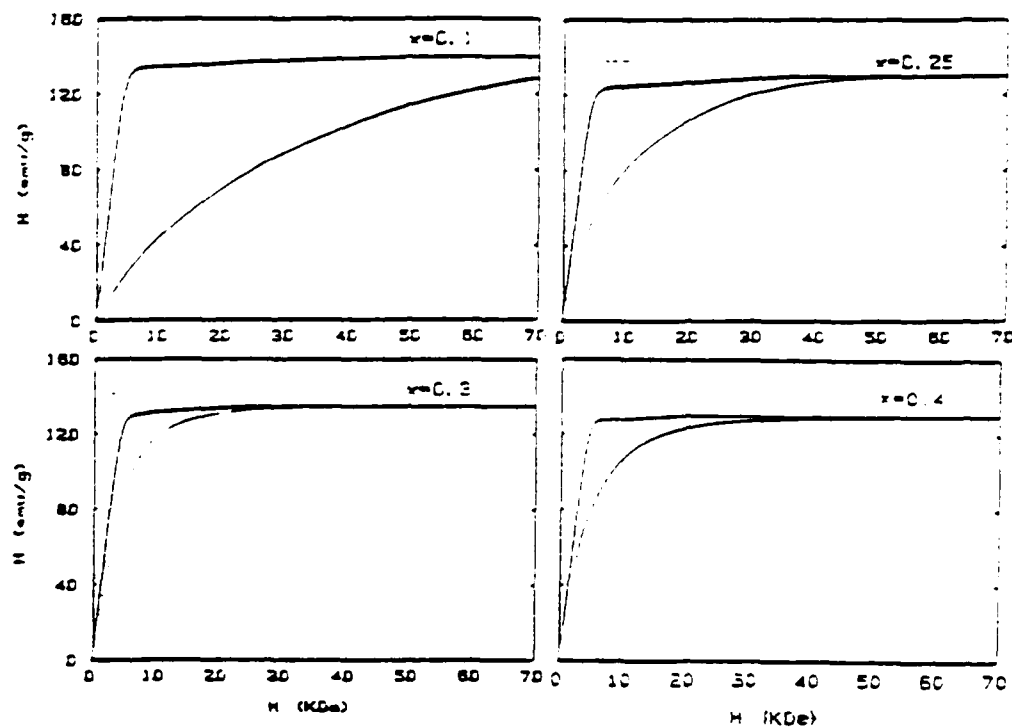Anisotropy field, easy magnetization direction and spin reorientation temperature of $(Nd_{1-x}Sm_x)_2Fe_{14}B$

| x | H_A(KOe) | E.M.D. | | T_s(K) |
	273K	1.5K	273K	
0.0	110	cone	axis	140
0.1	85	cone	axis	175
0.2	60	cone	axis	225
0.25	36	cone	axis	
0.3	very weak			
0.4		plane	plane	
0.5		plane	plane	
1.0		plane	plane	

Spin reorientation temperatures T_s increase with substitution of Nd by Sm and decrease with substitution of Nd by Pr. These results can be explained on basis of different sign of the second order Stevens factors. Sm has an opposite sign in comparison with that of Nd, while Pr has the same sign as Nd.

The substitution of Nd by Sm results in a continual decrease of uniaxial anisotropy at room temperature and an increase of spin reorientation temperature. This fact may be useful for some potential applications.

VII. MAGNETIC STRUCTURE OF DyFe$_3$

A. INTRODUCTION

DyFe$_3$, like all RFe$_3$ compounds, crystallizes in the PuNi$_3$ structure type, space group R3m.

The magnetic properties of DyFe$_3$ have been studied by Hoffer and Salmans [50], Van der Goot and Buschow [51], and others. DyFe$_3$ is ferrimagnetic with a Curie temperature considerably above room temperature, 605K.

The magnetic structures of RFe$_3$ intermetallic compounds including YFe$_3$ [52], HoFe$_3$ [53], TbFe$_3$ [54], and ErFe$_3$ [55,56] have been studied using neutron diffraction. Mossbauer spectra of DyFe$_3$ have been analyzed by Arif et al [57] Tsai et al [58], and Narasimhan et al [59], and it was suggested by Arif et al that Fe moments in DyFe$_3$ at 77K magnetize in the a-c plane at approximately 26° out of the basal plane.

We have carried out powder neutron diffraction studies of DyFe$_3$ and in this paper report on the nature of the magnetic structure.

B. EXPERIMENTAL

The crystalline samples of DyFe$_3$ were prepared by induction melting of the appropriate stoichiometric amounts of the elements in a cold boat crucible under an Ar atmosphere. A sample was annealed at 1000°C for 40 hours and then examined by X-ray powder diffraction. No lines of other phases were detected.

The neutron diffraction data were collected on a five detector diffractometer at the National Bureau of Standards Reactor using a wavelength of 1.55A. Soller slit collimators of angular divergences 10',20',10' were used before and after the monochromator and before the detector. The sample

container employed a flat plate geometry because of the high absorption of Dy for thermal neutrons. Appropriate absorption and geometrical corrections were made and the refinements were carried out using a modified Rietveld profile program [60]. The magnetic form factors for the Fe atom were taken from the literature [6], and those of Dy were calculated according to Stassis et al [61]. Nuclear scattering lengths of 1.69 and 0.96 were taken for the Dy and Fe atoms, respectively.

C. RESULTS AND DISCUSSION

The crystal structure of $DyFe_3$ will be described in the hexagonal form. In the unit cell of the structure, Dy atoms occupy two crystallographically nonequivalent sites $3a(Dy_I)$ and $6c(Dy_{II})$; Fe atoms occupy three nonequivalent sites $3b(Fe_I)$, $6c(Fe_{II})$, and $18h(Fe_{III})$.

At both 4 and 295K, the neutron diffraction patterns show the presence of a (003) peak indicating that the magnetic moments are not aligned along the c-axis and have a component of moments in the basal plane. The nuclear scattering of $DyFe_3$ does not make any contribution to the (003) peak.

In the powder profile fitting, in order to avoid non unique values of the highly correlated Fe moments, we assumed the Fe moments on the nonequivalent sites to be parallel and of equal magnitude, and allowed the Fe, Dy_I, and Dy_{II} moments to rotate in the a-c plane. We found that this noncollinear model gave a satisfactory fit to the data measured at and below room temperature. Rotation of individual Fe or Dy_I or Dy_{II} moments around the c-axis, constraining the others to the a-c plane, did not improve the fit.

The crystal and magnetic structure data are listed in Table XXI, and the latter are schematically shown in Figure 20. At 4K, the Fe moments are oriented 253.6° to the c-axis, the Dy_I and Dy_{II} moments lie at 71.8 and 51.5°

74

to the c-axis. The magnitudes of the Dy moments are close to the free ion values (10.0 μ_B), and the Fe moment near the elemental value of 2.2 μ_B. Within the limits of error the Dy moments on the two nonequivalent sites are the same. At 295K, the Dy moments are significantly reduced, whereas the Fe moments are nearly the same as expected. At room temperature all moments lie close to the basal plane. The magnetization per formula unit, 3.8 μ_B, calculated from the moments of DyFe$_3$ at 4K, is in good agreement with the observed value, 3.74 μ_B [51].

Arif et al [57] studied the Mossbauer spectrum of DyFe$_3$ at 77K, and suggested that the Fe moments at 77K lie in the a-c plane at approximately 26° out of the basal plane which is significantly different from our values of 16.4 and 12.2° out of the basal plane at 4 and 295K, respectively.

From Figure 20 it can be seen that the easy direction of Dy$_{II}$ lies closer to the c-axis than that of Dy$_I$. Under the competing interactions of exchange and crystal field interactions, the Dy moments assume the positions shown with the Fe moments coupled antiferromagnetically to the Dy and oriented along an intermediate direction. The rotation of moments as the temperature is raised can be accounted for by the reduction in second, fourth, and sixth order crystal field terms which have different temperature dependences.
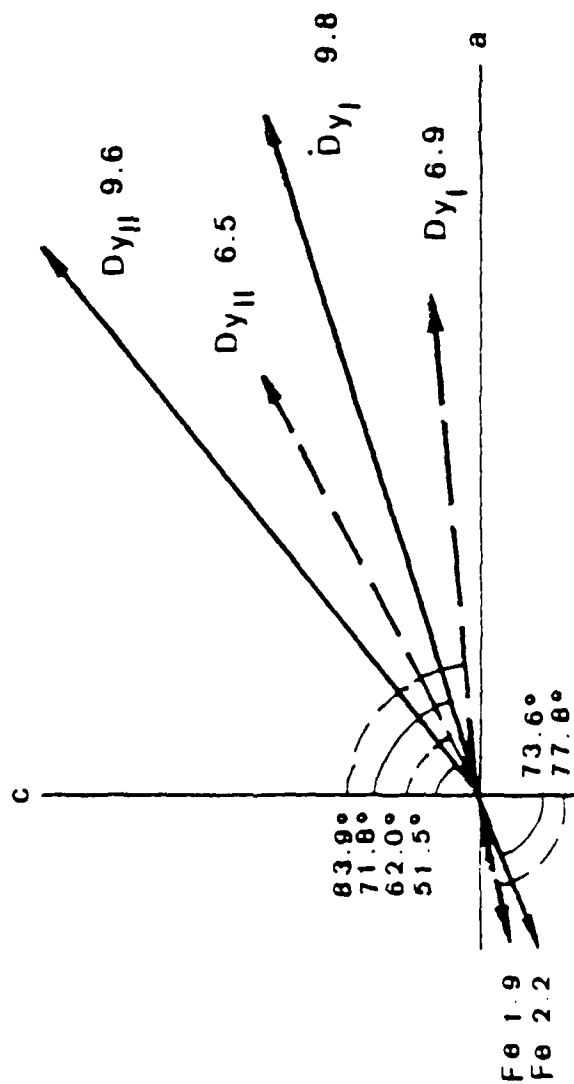
Figure 20. Magnetic moments (in μ_B) for DyFe$_3$ at 4 and 295K.

——— moments at 4K

- - - - moments at 295K

TABLE XXI

Crystal and magnetic structure data for $DyFe_3$.

Space group: R3m; Structure type: $PuNi_3$, hexagonal indexing.

	4K		295K	
	$|M|(\mu_\beta)$	$\theta(M,c)$	$|M|(\mu_\beta)$	$\theta(M,c)$
Dy_I	9.8**	71.8°***	6.9**	83.9°***
Dy_{II}	9.6	51.5°	6.5	62.0°
Fe	2.2	253.6°	1.9	257.8°
a(Å)	5.115		5.125	
c(Å)	24.508		24.578	
χ^*	1.37		1.27	
$\chi_{nucl.}$	0.83		1.13	
$\chi_{magn.}$	2.14		1.62	

$*\chi - R_{weighted}/R_{expected}$; etc.

**Moments in units of Bonr magnetrons, $\pm 0.2 \mu_3$

***$\pm 0.5°$

LIST OF PUBLICATIONS

1. R. J. Gan, N. T. Littlewood, and W. J. James, "Magnetic Structure of $Y_6(Fe_{1-x}Al_x)_{23}$", IEEE Transactions on Magnetics, Vol. Mag - 21, No. 5 1984 (1985).

2. N. T. Littlewood, W. J. James, and W. Yelon, "Magnetic and Crystallographic Structure of $Ho_6Mn_{23}D_{22}$", J. Magnetism and Magnetic Materials, $\underline{54-57}$, 491 (1986).

3. N. T. Littlewood, W. J. James, and W. Yelon, "Magnetic Structure of Ho_6Mn_{23}" submitted to J. Less-Common Metals (1986).

4. D. E. Tharp, G. J. Long, and W. J. James " A Mossbauer Effect Study of Magnetic Ordering in the $Y_6(Fe_xMn_{1-x})_{23}$ Solid Solutions", Hyperfine Interactions, $\underline{28}$, 593 (1986).

5. L. Jin, W. J. James, R. Lemaire and J. J. Rhyne, "Magnetic Structure of $DyFe_3$", J. Less-Common Metals, in press (1986).

6. L. Jin, W. J. James, R. Lemaire and J. J. Rhyne, "Magnetic Structure of $DyCo_3$", The Rare Earths in Modern Science and Technology", Vol. 5, in press (1986).

7. Y. C. Yang, W. J. James, H. Y. Chen and H. Sun, "Magnetocrystalline Amsotropy of $(Nd_{1-x}Sm_x)_2Fe_{14}B$ and $(Nd_{1-x}Pr_x)_2Fe_{14}B$", J. Magnetism and Magnetic Materials $\underline{54-57}$, 895 (1986).

8. Y. C. Yang, L. G. Yu, X. D. Li and W. J. James, "Magnetic Properties of Substituted $R_2(Fe,Al,Co)_{14}B$ Compounds", Transactions on Magnetics, in press (1986).

IX. PARTICIPATING SCIENTIFIC PERSONNEL

A. <u>Principal Investigator</u>: William J. James - Professor of Chemistry and Senior Investigator, Graduate Center for Materials Research.

B. <u>Co-Investigator</u>: Gary Long - Professor of Chemistry, Chemistry Department.

C. <u>Graduate Research Assistants</u>:

    (1) Tamara Littlewood - Ph.D., Chemistry earned 1986

    (2) Dwayne Tharp - candidate for Ph.D. in Chemistry

    (3) J. H. Han - candidate for Ph.D. in Chemistry

    (4) W. M. Sun - candidate for Ph.D. in Chemistry

*D. <u>Dr. R. Lemaire</u> - Néel Laboratory CNRS, Grenoble, France

    <u>Dr. Y. C. Yang</u> - Professor of Physics, Peking University, Peoples Republic of China

    <u>Dr. W. B. Yelon</u> - Professor of Physics, University of Missouri Research Reactor, UMC

    <u>Dr. J. Rhyne</u> - Reactor Radiation Division, NBS, Washington, D.C.

*Above did not receive salaries or support from contract but did assist, and interact with, the graduate students and principal investigator.

REFERENCES

1. K. Hardman, Ph.D. Thesis, University of Missouri - Rolla (1979).

2. K. Hardman, W. J. James, J. Deportes, R. Lemaire, R. P. delaBathie, J. de Physique, C5 $\underline{40}$,204 (1979).

3. F. Pourarian, E. B. Boltich, W. E. Wallace, R. S. Craig and S. K. Malik, J. Mag. Magn. Mat., $\underline{21}$, 128 (1980).

4. W. C. Koehler, J. W. Cable, M. K. Wilkinson and E. O. Wollan, Phys. Rev., $\underline{151}$, 414 (1966).

5. C. G. Shull and E. O. Wollan, Solid State Physics, vol. 2, Academic Press, New York (1956).

6. G. E. Bacon, Neutron Diffraction 3rd ed., Clarendon Press, Oxford (1975), p277.

7. A. Delapalme, J. Deportes, R. Lemaire, K. Hardman and W. J. James, J. Appl. Phys., $\underline{50}$, 1987 (1979).

8. K. Hardman, W. J. James and W. Yelon, The Rare Earths in Modern Science and Technology vol 1, Plenum, New York, 1978.

9. M. J. Cooper, Acta. Cryst., A$\underline{38}$, 264 (1982).

10. W. Schafer and G. Will, J. Less-Common Metals, $\underline{94}$, 205 (1983).

11. J. R. Chamberlain, Physica, $\underline{86-88B}$, 138 (1977).

12. K. Hardman, J. J. Rhyne, S. Malik and W. E. Wallace, J. Appl. Phys., $\underline{53}$ 1944 (1982).

13. R. J. G. Tompson, H. W. White, B. Kebe and W. J. James, J. Chem. Phys. $\underline{78}$ 7502 (1983).

14. J. J. Rhyne, G. E. Fish, S. G. Sankar and W. E. Wallace, J. de Physique, C5 $\underline{40}$, 204 (1979).

15. K. Hardman-Rhyne, J. J. Rhyne, E. Prince, C. Crowder and W. J. James, Phys. Rev., B. $\underline{29}$, 416 (1984).

16. K. Hardman, J. J. Rhyne, H. K. Smith and W. E. Wallace, J. Less-Common Metals, $\underline{74}$, 97 (1980).

17. J. J. Rhyne, K. Hardman-Rhyne, H. K. Smith and W. E. Wallace, J. Less-Common Metals, $\underline{94}$, 95 (1983).

18. P. C. Bouton and A. R. Miedema, J. Less-Common Metals, $\underline{71}$, 147 (1980).

19. I. Jacob, J. M. Bloch, D. Shaltiel and D. Davidov, Solid State Comm., $\underline{35}$, 155 (1980).

20. I. Jacob, Solid State Comm., 40, 1015 (1981).

21. D. G. Westlake, J. Less-Common Metals, 75, 177 (1980).

22. D. G. Westlake, H. Shaked, P. R. Mason, B. R. McCart, M. H. Mueller, T. Matsumoto and M. Amaro, J. Less-Common Metals, 91, 1 (1983).

23. D. G. Westlake, Scripta Metallurgica, 16, 1049 (1983).

24. D. G. Westlake, J. Mat. Sci., 18, 605 (1983).

25. D. G. Westlake, J. Less-Common Metals, 90, 251 (1983).

26. C. Crowder, Ph.D. Thesis, University of Missouri - Rolla (1982).

27. R. A. Young, E. Prince and R. A. Sparks, J. Appl. Crys., 15, 357 (1982).

28. C. Crowder, B. Kebe, W. J. James and W. B. Yelon, AIP Conf. Proc., 39, 318 (1982).

29. H. Oesterreicher, Appl. Phys., 24, 169 (1981).

30. M. Commandre, D. Fruchart, A. Rouault, D. Sauvage, C. B. Shoemaker and D. P. Shoemaker, J. Phys. Lett., 40, L639 (1979).

31. S. K. Malik, T. Takeshita and W. E. Wallace, Solid State Communications, 23, 599 (1977).

32. D. Givord and R. Lemaire, J. Physique 32, (C1-6), 668 (1971).

33. W. J. James, K. Hardman, W. Yelon and B. Kebe, J. de Physique, C5, 206 (1979).

34. K. Hardman, J. J. Rhyne and W. J. James, J. Appl. Phys. 52, 2049 (1981).

35. K. Hardman, W. J. James and W. B. Yelon, J. Phys. Chem. Solids 41, 1105 (1980).

36. M. J. Besnus, J. M. Bouton and R. Clad, Phys. Stat. Solids, 53, 351 (1979).

37. W. E. Wallace in Rare Earth Intermetallics, (Academic Press, Inc., New York, 1973) p. 187.

38. C. E. Crowder and W. J. James, J. Less Common Metals 95, 1 (1983).

39. H. R. Kirchmayr and W. Steiner, J. Physique 32, C1-665 (1971).

40. G. J. Long, K. Hardman and W. J. James, Solid State Comm., 34, 253 (1980).

41. J. V. Florio, R. E. Rundle and I. A. Snow, Acta Cryst., 5, 449 (1952).

42. M. Sagawa, S. Fujimura, H. Yamamoto, Y. Matsuure, and K. Hiraga, IEEE Trans. Magn., MAG-20, 1548 (1984).

43. Y. C. Yang, W. W. Ho, H. Y. Chen, J. Wang, and J. Lan, J. Appl. Phys., 57, 4118 (1985).

44. W. Sucksmith and J. E. Thompson, Proc. Roy. Soc., A225, 362 (1954).

45. J. J. Herbst, J. J. Croat, F. E. Pinkerton, and W. B. Yelon, Phys. Rev., B29, 4176 (1984).

46. J. D. Livingston, J. Appl. Phys., 57, 2544 (1981).

47. M. Sagawa, S. Fujimura, M. Togawa, H. Yamamoto and Y. Matsuura, J. Appl. Phys., 55, 2083 (1984).

48. D. Givord, H. S. Li and R. Perrier de la Bathie, Sol. Stat. Commun., 51, 857 (1984).

49. Ying-chang Yang, Hai-ying Chen, Zun-xiao Liu, Bing Liao, Feng Xing and Wen-wang Ho, J. Appl. Phys., 57, 4118 (1985).

50. G. I. Hoffer and L. R. Salmans, Proc. 7th Rare Earth Research Conference, Carnado, California, 371 (1968).

51. A. S. Van der Goot and K. H. J. Buschow, J. Less-Common Metals, 21, 151 (1970).

52. E. Burzo and F. Givord, Compt. Rend. Sci, Paris, 271, 1159 (1971).

53. M. Simmons, J. M. Moreau, and W. J. James, J. Less-Common Metals, 30, 75 (1973).

54. W. J. James, K. Hardman, W. Yelon, J. Keem, and J. Croat, J. Appl. Phys., 50, (3) 2006 (1979).

55. R. L. Davis, R. K. Day, and J. P. Dunlop, J. Phys, F: Metal Phys., 7, (9) 1885 (1977).

56. B. Kebe, W. J. James, J. Deportes, R. Lemaire, W. Yelon, and R. K. Day, J. Appl. Phys., 52, (3) 2052 (1981).

57. S. K. Arif, D. St. P. Bunbury, G. J. Bowden, and R. K. Day, J. Phys. F: Metal Phys., 5, 1048 (1975).

58. S. C. Tsai, K. S. V. L. Narasimhan, C. J. Kinesh, and R. A. Butera, J. Appl. Phys., 45, 3582 (1974).

59. K. S. V. L. Narasimhan, R. A. Butera, and R. S. Craig, J. Phys. Chem. Solids, 34, 1075 (1973).

60. H. M. Rietveld, J. Appl. Cryst., 2, 65 (1969).

61. C. Stassis, H. W. Deckman, B. N. Harmon, J. P. Desclaux, and A. J. Freeman, Phys. Ref. B, 15, 369 (1977).

END

DTIC

7 — 86